Integrated Microfluidic System for Digital Detection of Extracellular Vesicles

By

Gopi Chandran Ravichandran
B.E., Anna University, 2017

Submitted to the graduate degree program in Bioengineering and the Graduate Faculty of the University of Kansas in partial fulfillment of the requirements for the degree of Master of Science.

_____

Chair: Dr. Yong Zeng

_____

Dr. Candan Tamerler

_____

Dr. Prajna Dhar

Date Defended: 2 June 2020

The thesis committee for Gopi chandran Ravichandran certifies that this is the approved version of the following thesis:

Integrated Microfluidic System for Digital Detection of Extracellular Vesicles

Chair: Dr. Yong Zeng

Date Approved: 2 June 2020

Abstract

Investigating the components of extracellular vesicles (EV) has shown substantial promise for cancer diagnosis. However, detecting them individually and profiling its membranal proteins is still challenging. Isolating EVs individually can help us track their protein expression and to study their heterogeneity. We propose a microfluidic platform for capture of EVs and digitally detect them with the help of a digital microarray and a smart actuation device for sealing the microwells. The chip achieves the EV quantification by digital Enzyme-Linked Immunosorbent Assay (ELISA) and enzymatic signal amplification. Specific areas of glass slide beneath the detection area of the chip coated with anti-CD81 antibodies are used to capture EVs. A cocktail mixture of biotin-labeled anti-CD9 and anti-CD63 antibodies were used as detection antibodies to detect the captured EVs. Enzymatic amplification of the detection signal was achieved with the help of Streptavidin Beta Galactosidase (SßG) as a reporter enzyme and Fluorescein-di-ß-D-galactopyranoside (FDG) as a substrate. A closed-loop actuator device that is controlled by a microcontroller using the feedback from a force sensor was developed to seal the microwell array to conduct discrete enzymatic reactions for digital quantification of single captured targets. An automatic image processing algorithm in MATLAB has been developed for digital signal image analysis. It automatically detects individual microwells and determines the average intensity of each microwell by calculating the average of intensities around the center of the microwell. The digital detection and quantification of captured EVs were achieved. Automation was incorporated in sealing and analyzing images, which makes it closer to fully automated microfluidic systems in the future.

Acknowledgement

I would like to thank my advisor, Dr. Yong Zeng for his support and mentorship throughout my journey as a graduate student. His ideas and strategies for problem-solving have inspired me a lot and has taught me to implement them in real life. I am grateful for the time he has spared for me and the constant motivation from him. I would also like to thank my committee members, Dr. Candan Tamerler and Dr. Prajna Dhar for their continuous encouragement and assistance. I am very much thankful for their time and dedication.

I would also like to thank my colleagues of the past and present in our research group, Xin Zhou, Yang Yang, Yahoa Zhang, Dr. Peng Zhang, and Dr. Yutao Li.

Finally, I would like to thank my family members and friends for their emotional support and encouragement throughout my journey.

Table of Contents

Abstract iii

Acknowledgement iv

List of Figures vii

List of Tables x

1. Introduction 1

1.1. Background and Significance 1

1.2. Extracellular Vesicles for Cancer Diagnosis 2

1.3. Microfluidic Lab-on-a-chip Technology 3

2. Enzyme Linked Immuno-Sorbent Assay (ELISA) 10

2.1. ELISA Principle 11

2.2. Types of ELISA 11

2.3. Digital ELISA 12

3. Automation in Digital Signal Acquisition and Image Analysis 16

3.1. Closed Loop System 16

3.2. Force Sensitive Resistor (FSR) 16

3.3. Image Processing 17

3.3.1. Hough Transform 17

3.3.2. Contrast Enhancement 19

4. Experimental Methods 20

4.1. Reagents and Materials 20

4.2. Design and Microfabrication of Microfluidic Chip 20

4.3. Microfluidic Pumping and Inter-channel Leakage Test 22

4.4. Building Closed-loop Actuator System 23

4.5. Connection of Closed-loop Actuator System 26

4.6. Determining Set Point Force Range for Actuator System 27

4.7. Photobleaching Experiment 27

4.8. Free Enzyme Assay 27

4.9. Comparison of PLL and APTES for Surface Patterning 28
4.10. Quantification of Total Extracellular Vesicles present using Digital ELISA 29
4.11. Automated Analysis of Digital Microwell Images using an Image Processing Algorithm 31
4.12. Algorithm Testing for Accuracy and Precision of Microwell Detection 33
5. Results and Discussion 34
5.1. Design and Microfabrication of Microfluidic Chip 34
5.2. Microfluidic Pumping and Inter-channel Leakage Test 36
5.3. Building Closed-loop Actuator System 37
5.4. Set Point Force Range for Actuator System 38
5.5. Photobleaching Experiment 39
5.6. Free Enzyme Assay 40
5.7. Efficiency and Precision of MATLAB Algorithm for Microwell Detection 42
5.8. Comparison of PLL and APTES for Surface Patterning 43
5.9. Quantification of Total Extracellular Vesicles Present using Digital ELISA 44
6. Conclusion and Future Work 48
6.1. Conclusion 48
6.2. Future Work 48
6.2.1. Standalone Integrated System 48
6.2.2. Digital ELISA 49
6.2.3. Detecting Tumor Associated Molecules inside EV 49
7. Appendix 51
7.1. Arduino Code for Closed-loop Actuator 51
7.2. MATLAB Code for Detecting and Analyzing Circles 52
7.3. Detection and Analysis of Square Microwells 54
Reference 58

List of Figures

Figure 1: Extracellular vesicles' properties(a) Schematic representing EV composition and (b) Level of circulating markers in blood during various stages of cancer [7]. 3

Figure 2: A microfluidic chip with nano-Herring bone structures fabricated with silica beads for efficient capture of EVs [4]..... 4

Figure 3: Structures and reaction involved in PDMS formation (a) Siloxane oligomer and (b) cross-linker of the PDMS base and curing agent respectively. (c) Cross-linking reaction between PDMS base and curing agent [19]. 6

Figure 4: Schematic of photolithography process (a) SU-8 photoresist coating on silicon water, (b) pattern is transferred into the photoresist by aligning mask over the photoresist, (c) the fabricated photoresist structure after washing with SU-8 developer, (d) pouring the PDMS on the master wafer to cast the features , and (e) the peeled PDMS is bound to another substrate like glass [24]. 8

Figure 5: : Schematic of PDMS casting procedure[26]. 10

Figure 6: : Illustration of direct, indirect, sandwich, and competitive ELISA[31]. 12

Figure 7: Different types of digital ELISA (a) Droplet array based digital ELISA[32], (b) Single molecule array technology in fiber optic cable[33], (c) Isolation of reagents into PDMS compartments for analysis[34], (d) Digital ELISA on captured targets on substrate[5]. 14

Figure 8: : Force Sensitive Resistor and its properties (a) A square FSR sensor and (b) Graph showing relationship between the applied force and resistance[37]. 17

Figure 9: Representation of (a) an example of candidate pixel in an actual circle (solid) and accumulator array votes and (b) finding center of the circle[39]..... 18

Figure 10: Representation of (a) low and (b) high contrast image. 19

Figure 11: Schematic illustration of the design of a three-layer PDMS/Glass chip that has an eight-valve system, lysis and detection chambers..... 22

Figure 12: Design of the actuator setup with FSR..... 24

Figure 13: Schematic explanation of (a) Workflow of the closed loop actuation system. (b) Algorithm of the Arduino code. 25

Figure 14: Circuit connection of the closed loop actuation system 26

Figure 15: Schematics explaining digital signal acquisition (a) Before sealing the microwells onto the glass slide, (b) After sealing to produce digital signal. 28

Figure 16: Schematic of the workflow of Digital ELISA protocol. EVs were captured using immobilized capture Abs. Then using the biotin labelled detection antibody and the reporter enzymes SßG they were digitally detected. 29
Figure 17: Workflow of the automated image analysis (a) Microwells detected by the algorithm. (b) Illustration of a negative (left) and a positive (right) microwells, showing the area (red square) considered for calculating the average intensity. (c) Histogram showing number of microwells at each intensity value. (d) Screenshot of MATLAB command window showing the output of number of positive microwells. 31
Figure 18: Final microfabricated (a) master wafer for fluidic layer, (b) master wafer for pneumatic layer, (c) PDMS chip after aligning fluidic layer and pneumatic layer and then bonded to glass slide. 35
Figure 19: Inter-channel (a) Setup showing food dye and water in two inlets to test inter channel leakage. (b) Final image taken after the test showing no inter-channel leakage. 37
Figure 20: Final connected closed loop actuation system with actuator, Arduino microcontroller, and FSR. 37
Figure 21: Graph showing the probability of breakage vs the force sensed on the FSR to determine the breaking threshold. 38
Figure 22: Images taken at 20-minute interval to test for any diffusion of dye into the photobleached area. 39
Figure 23: Digital microwell resultant image taken after (a) 10 min and (b) 20 min. 41
Figure 24: Accuracy determination of algorithm (a) Blank PDMS image used as negative control, (b) Microarray image showing detected microwells. 42
Figure 25: Resultant graph representing detected microwells in negative control, microarray, and total microwells present. 43
Figure 26: Bar plots showing the comparison of background and signal for detection of 10µg/ml of exosomes captured in (a) APTES and (b) PLL modified glass slide. 44
Figure 27: Example of an individual image out of 16 images, covering entire microwell array and their corresponding MATLAB outputs for the entire microarray for (a) Negative control, (b) 10µg/ml (1:100), and (c) 100µg/ml (1:10). 46
Figure 28: Comparison of log% positive wells vs log concentration of exosomes. 47

Figure 29: Visualization of the assay protocol using food dyes. (A) Capture of the exosome captured magnetic beads in the lysis chamber. (B) Introduction of the 0.1 µl of lysis buffer(red dye) into the lysis chamber. (C) Dilution of the lysate with dilution buffer(green dye). (D) After dilution of lysate to 0.2 µl. (E) Pumping of the lysate to the detection chamber where capture probes will be immobilized to captute target molecules. (F) Washing the lysate with washing buffer before introducing detection probes. 50
Figure 30: Image showing detected squares in a microarray with square shaped microwells. 57

List of Tables

Table 1: Delay set to achieve specific flow rates for various reagents involved in the assay. 36

1. Introduction

1.1. Background and Significance

Cancer has been one of the most convoluted and challenging diseases of medical history. It has been a major problem throughout the world and is the second-highest cause of death in the United States[13]. By the end of 2020, it has been projected that 1,806,590 new cancer cases and 606,520 cancer deaths are expected in the United States. Apart from finding the right treatment to cure the disease, finding diagnostic and prognostic tools are also critical to reduce the death rate. Late diagnosis and poor prognosis due to the disease's intricacy could lessen the success rate of curing cancer[14]. Thus, highly sensitive diagnostic approaches for early-stage, advanced stage, and during treatment to monitor the efficacy of a drug is critical to reducing the mortality rate. Early-stage cancer detection can play a vital role in improving cancer survival rate, recovery rate, and avoiding the recurrence of cancer[15]. Rapid advancements in early-stage diagnosis and precision therapy for cancer has been happening for years[1]. This has amplified the demand for ultrasensitive detection of disease-related elements in human biological samples. This technique is called the liquid biopsy and is a non-invasive alternative for tissue biopsy[12]. It has a promising potential for clinical disease diagnosis, the progression of the treatment, and survival prediction of patients[16]. As extracellular vesicles (EV) that are tumor-derived have been found in biological samples, they can serve as a potential target during the liquid biopsy. Thus, there has been an increasing significance in developing ultrasensitive technologies to meet the demand of exosome research and clinical applications.

1.2. Extracellular Vesicles for Cancer Diagnosis

Exosomes are a subcategory of extracellular vesicles (EVs) which are 30-150nm in size[16]. It is secreted in biological fluids by most eukaryotic cells. In cancer patients, it has been found to accumulate in human blood and malignant discharges[1]. It has been found that they play a vital role in cell communication, tumorigenesis, metastasis, and immune responses by transporting several effectors or signaling molecules such as RNA, antigens, and contagious particles[16]. These enriched genetic material and proteins containing information about their cellular origin, are stably carried by these EVs, thereby holding great potential for early-stage cancer diagnosis (Figure 1a). Therefore, they have been targeted by many researchers to improve liquid biopsy technology for non-invasive cancer diagnosis. Circulating tumor cells have also been a target for liquid biopsy[6]. But due to their less concentration in blood (1-10/ml of blood) compared to the exosomes ($>10^9$ vesicles/ml of blood, EVs have become a better surrogate in liquid biopsy (Figure 1b). It has been demonstrated in various researches that EVs can be isolated from many bodily fluids namely, blood plasma, serum, saliva, breastmilk, urine, bronchial lavage fluid, amniotic fluid, cerebrospinal fluid, and malignant ascites[17]. Commonly, the analysis of microRNAs (miRNAs) and proteins present inside or outside EVs are done for EV characterization[15]. And it is achieved by conventional methods like real-time PCR, enzyme-linked immunosorbent assay (ELISA), Western blotting, and mass spectroscopy. The shortcomings of these types of analytical procedures are that they typically involve tedious and laborious sample pretreatments such as ultracentrifugation and size-exclusion chromatography. Moreover, the analysis techniques itself possess several disadvantages like poor sensitivity, time-consuming, and large sample consumption[1]. Also, forced filtration and shearing force involved in these techniques can lead to

EV membrane fusion and loss of integrity[6]. Microfluidic lab-on-a-chip technology has lately been an efficient and promising alternative for exosome isolation and analysis.

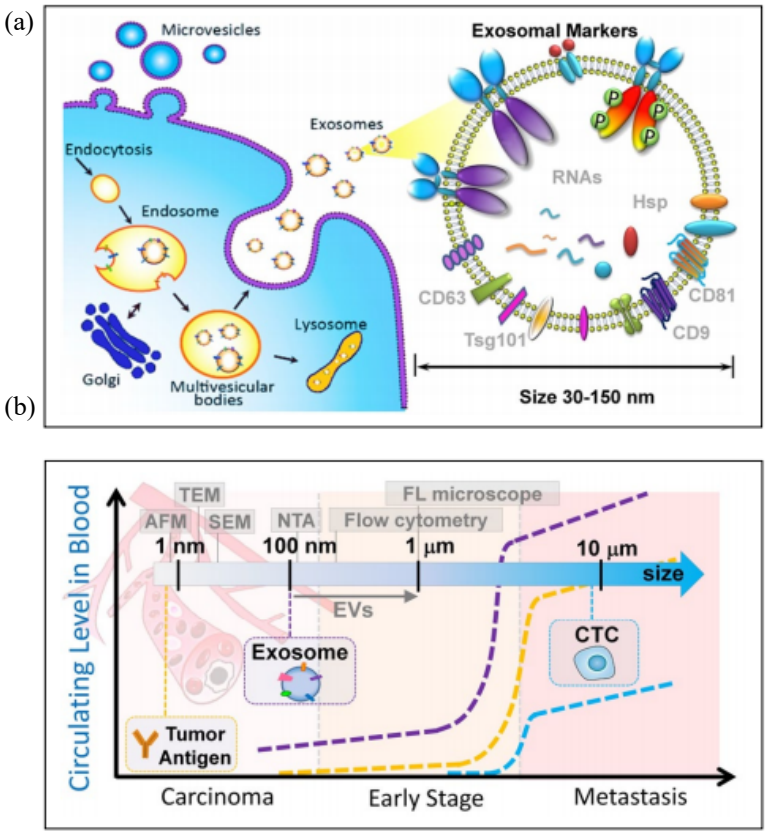

Figure 1: Extracellular vesicles' properties(a) Schematic representing EV composition and (b) Level of circulating markers in blood during various stages of cancer [6].

1.3. Microfluidic Lab-on-a-chip Technology

The concept of microfluidic technology as its name suggests is based on drastically reducing the scale of experimentation. Recently it has become a ubiquitous technology for cancer-related research[18]. The benefits that they possess are smaller volumes of reagents involved in the experiment thereby reducing the cost and waste produced, giving a larger surface to volume ratio, and increasing speed, accuracy, and sensitivity (Figure 2). As the dimensions involved are on a small scale, it can reduce the diffusion times and thereby result in the faster analysis[19]. And

because the requirement of valuable reagents and samples to execute the experiment has reduced, it lowers the cost involved per assay.

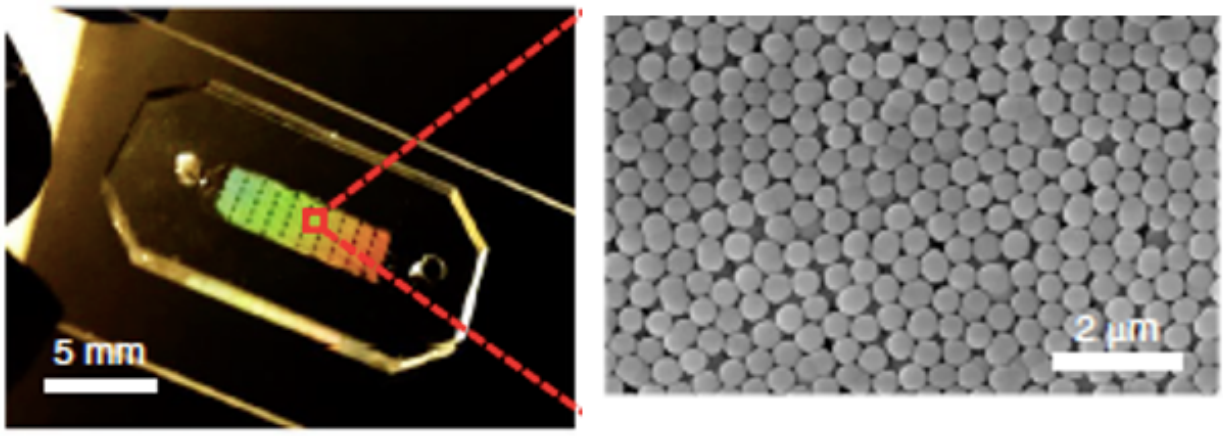

Figure 2: A microfluidic chip with nano-Herring bone structures fabricated with silica beads for efficient capture of EVs [1].

In microfluidic chips, the fluid mostly exhibits a laminar flow, where the fluid streams will flow parallel to each other and Reynold's number is less than 2300[20]. And at such smaller scales, diffusion is the dominant means for lateral mixing. Compared to the macroscale setup where fluid transport mostly occurs by inertial forces, viscous forces are what govern the fluid movement in microfluidics[21]. The microscale advantage enables the control of physics, chemistry and, physiology at the cellular level. Microfluidics can be in two primary forms namely, channel microfluidics and droplet microfluidics[22]. In channel microfluidic systems, microscale channels and chambers are involved and the flow is predominantly laminar. Whereas in droplet microfluidic systems, immiscibility of water and oil is used to create pico-liter and nanoliter droplet microreactors. Channel microfluidic devices have been fabricated with materials such as silicon, etched glass, or elastomers which makes them more biocompatible and inexpensive. They are then bonded to glass for usage. Recently paper-based microfluidic devices have also been emerging[23, 24]. In the field of cancer research, microfluidics has been playing a critical role in cancer cell

isolation, molecular diagnostics, understanding tumor biology, and high-throughput screening for therapeutics[25]. By developing and using state of art microfluidic technologies, unmet challenges in disease management and patient care can be addressed.

1.3.1. Polydimethylsiloxane as the Material for Microfluidic Chips

Polydimethylsiloxane (PDMS) is a silicone-based elastomer that is ubiquitously used in microfluidics[26]. Fabrication with PDMS is very quick, easy, easy to integrate with glass slides, and is capable of nano-level replication of structures. In addition, due to its optical transparency, it makes real-time monitoring of the microchannels possible and its low autofluorescence property benefits during fluorescence imaging. Excellent biocompatibility and permeability are also other properties that give a helping hand for various microfluidics-based research. Even though PDMS has these convincing advantages they also possess significant disadvantages. Specifically of microfluidic applications adsorption of molecules is possible, and it can get intensified at a favorable pH[27]. Hydrophobicity, evaporation due to permeability, and swelling is hydrocarbon-based solvents are other shortcomings that PDMS possess. Plasma treatment on PDMS can introduce polar functional groups (SiOH) and can modify the surface temporarily to hydrophilic. Although PDMS has certain drawbacks, its beneficial properties outweigh its disadvantages. Along with the above-mentioned advantages, the elasticity of PDMS is also significantly important for our application. The elasticity makes mechanical sealing of digital microwell array possible specifically for this application. PDMS is commercially available as a kit that comes with a base material and a curing agent[8]. They both comprise of siloxane oligomers terminated with vinyl groups. The base comes with a platinum-based catalyst that assists in the curing of the elastomer by forming Si-CH_2-CH_2-Si linkages (Figure 3). The properties of the resultant elastomer are

dependent on the ratio curing agent to base, the more the ratio the higher the rigidity of the elastomer.

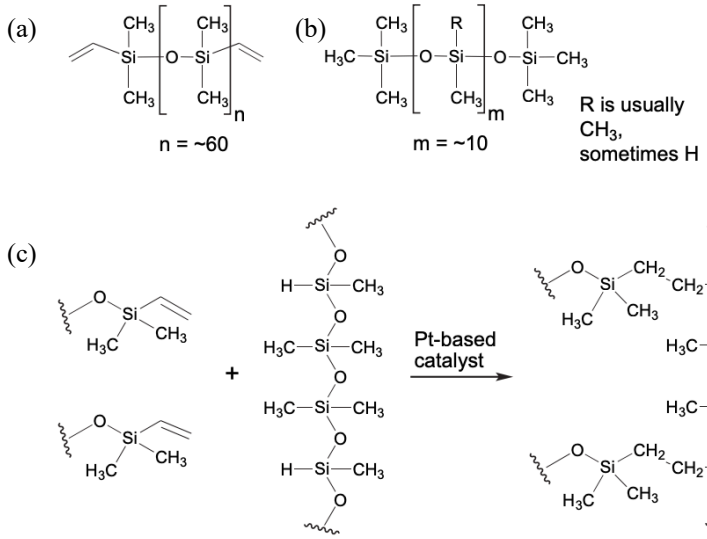

Figure 3: Structures and reaction involved in PDMS formation (a) Siloxane oligomer and (b) cross-linker of the PDMS base and curing agent respectively. (c) Cross-linking reaction between PDMS base and curing agent [8].

1.3.2. Microfabrication Technique

Microfabrication is an imperative contributor to technology. It has been widely used for sensors fabrication, microreactors, microelectromechanical systems (MEMS), microanalytical systems, and microreactors[28]. One of the most ubiquitous and powerful techniques of microfabrication is photolithography. This technique is capable of mass-producing features made of photoresists with a resolution of ~250nm. By employing a photomask, the entire pattern from it can be projected onto a thin light-sensitive photoresist film to create the patterned features. The mask only transmits the radiation where it is needed and blocks the radiation in unwanted regions. The patterns on the masks are designed using AutoCAD or TurboCAD software and are transferred onto the mask using lasers.

Photoresist

Photoresists are photoreactive polymers used in photolithography. They can be of two types based on how it chemically reacts to radiation namely, negative or positive photoresists[29]. The photoresists are comprised of three main components that are resin, photoactive compound, and solvent. Resin is a thermoplastic material responsible for creating those features in photolithography. Resin is capable of getting dissolved in a developer solution. The solvent is responsible to provide photoresists an ability to be coated on substrates by decreasing the viscosity of photoresist. It can evaporate from the photoresist during baking steps. The photoactive compound or the sensitizer is the light-sensitive component of the photoresist. It can alter its property to chemically resist developer solution when exposed to radiation at a particular wavelength. In the case of a positive photoresist, the pattern created will be the same as the mask. During exposure, the light will degrade the exposed regions of the polymer and make it more soluble in developer solutions which are mostly organic solvents. In the case of a negative photoresist, the pattern is the inverse of what the mask has. Light exposed areas undergo 3D cross-linking in the polymer structure, thereby strengthening its resistance to dissolution in the developer solution. Usually, the negative photoresist is a favored option because of its superior adhesion to silicon wafers that are used as substrates[30]. This adhesion is important for soft lithography when PDMS is cast using these molds and peeled off from it.

Photolithography

Silicon wafers used as a substrate for photoresist deposition needs to be primed before coating it with photoresist[31]. This can be done by baking it at 150ºC for 30 minutes making it undergo dehydration. It can significantly help in the coating of the hydrophobic photoresist. Another way

of doing this would be by immersing the wafers in piranha solution which is a mixture of concentrated sulfuric acid (H_2SO_4) and hydrogen peroxide (H_2O_2) at a ratio of 3:1. Hexamethyldisilazane (HMDS) can also be used as an adhesion promoter for photoresists. This can be achieved by vapor deposition or spin coating of HMDS on silicon wafers to make it hydrophobic.

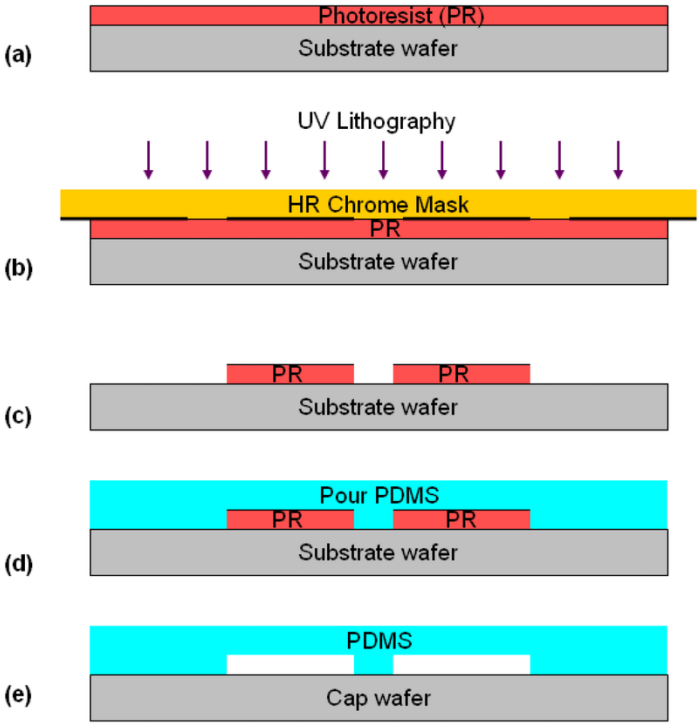

Figure 4: Schematic of photolithography process (a) SU-8 photoresist coating on silicon water, (b) pattern is transferred into the photoresist by aligning mask over the photoresist, (c) the fabricated photoresist structure after washing with SU-8 developer, (d) pouring the PDMS on the master wafer to cast the features , and (e) the peeled PDMS is bound to another substrate like glass [9].

Followed by the pretreatment photoresist is spin-coated onto the wafer (Figure 4a). The wafer is held onto the chuck at the center and held using a vacuum. The final thickness of the coating is dependent on numerous factors namely, the intrinsic viscosity of the photoresist, the concentration of the polymer in the photoresist, speed of the spin coater in rotations per minute (rpm)[30]. The film thickness decreases as the speed of rotation increases. After spin coating,

prebaking at 65ºC and 95ºC is done for a certain time interval to improve the adhesion of photoresist to a substrate and to get rid of the solvent. The time depends on the desired photoresist thickness. After letting it cool at room temperature, exposure is done at a particular wavelength with a mask in between (Figure 4b). Usually, a mercury arc lamp is used to create UV radiation at wavelengths 365nm, 405nm, or 436nm. The exposure dose is dependent on the desired resist thickness, more dose is needed for thicker films. The exposure time is directly proportional to the dose (mJ/cm^2) and inversely proportional to the power or light intensity (mW/cm^2). The dose is the amount of energy required to complete the exposure, and the power is the intensity of the UV light source which varies with wavelength. Exposure time is crucial to optimize as it can cause overexposure or underexposure and result in erroneous fabricated features. Overexposure can cause overproduction of hexafluoroantimonic acid in negative SU-8. Exposure can have effects on the photoresist depending on its type as discussed in the photoresist section above. The resolution of the features is dependent on the wavelength of the light used for exposure, the gap between the mask and substrate, and the thickness of the resist. Followed by the exposure, post-exposure baking is done in the case of negative photoresists only. The formation of the insoluble layer to the developer solution is completed after this step. It is also done as a two-step process at 65ºC and 95ºC for some time depending on film thickness. The next step would be development using SU8 developer (Figure 4c). The substrate is immersed into the developer solution and can be either swirled by hand, shaken in an orbital shaker or mega sonic agitation can be done based on the complexity of the features. Isopropyl alcohol can be used to wash the excess developer solution and then blow-drying it with nitrogen gas is done. Also, an optional hard baking step at 150-200ºC can be done for 30min to further cross-link resists improving structural stability.

PDMS casting

The photolithography process discussed above is used to produce master molds for PDMS casting. PDMS can be easily cast from the master mold, making the process of microfabrication easy and inexpensive (Figure 5)[5, 32]. Before pouring PDMS on to the master mold Hexamethyldisiazane (HMDS) or tricholor(1H,1H,2H,2H-perfluoroctyl) silane (PFOTS) are vapor-deposited to create hydrophobic monolayer to reduce adhesion of PDMS to the mold. As described in the PDMS section, the base material and the curing agent are mixed at a preferred ratio and poured onto the Si mold after degassing it, to remove air bubbles. Once heating is done at elevated temperatures for a few hours, the liquid mixture becomes a solid as described in the PDMS section. Then the cured PDMS can be cut and peeled off from the master mold.

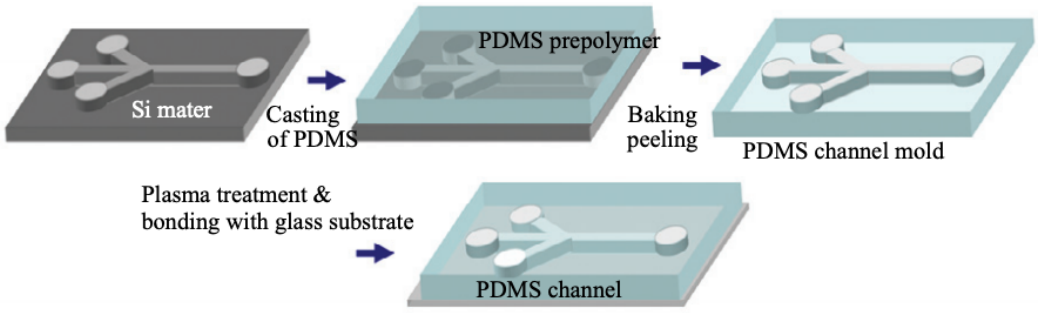

Figure 5: : Schematic of PDMS casting procedure[5].

2. Enzyme Linked Immuno-Sorbent Assay (ELISA)

ELISA is a ubiquitous technique used to measure the concentration of antigens or antibodies in biological samples[33]. ELISA can also be called as an immunosorbent assay. The technique is predominantly employed in medical laboratories, in vitro diagnostic product manufacturers, regulatory bodies, external quality assessment, and proficiency-testing organizations. It uses

specific antibodies covalently coupled with the enzyme. The amount of antigen present is determined by the amount of antibody binding to the antigen. Enzyme labels are used for the detection, and they are mostly alkaline phosphatase or horseradish peroxide. Change in color, emission of light, or any other signal are used to detect the analyte. This technique is mainly designed for detecting and quantitating peptides, proteins, antibodies, and hormones.

2.1.ELISA Principle

ELISAs are performed in 96-well or 384-well polystyrene plates[34, 35]. The antigen or antibodies with the required specificity are immobilized onto the solid surface. Then different biological samples are incubated in different wells. Positive and negative controls will also be incubated along with the samples. As the ELISA reactants are immobilized on the microplate, it makes it easy to separate bound substances from unbound ones. This ability to wash away nonspecifically bound materials makes this technique a powerful tool for measuring specific analytes. Wash buffer is used to eliminate the sample and unbound antibodies or antigens. Then secondary antibodies linked with enzymes are added to each well and incubated to yield a detectable product. The specificity of the antibody-antigen interaction is very crucial. The detection enzyme may either be attached directly to the primary antibody or may be introduced with a secondary antibody. Linking with a protein like streptavidin is also possible when the antibody is biotin-labeled.

2.2. Types of ELISA

Based on the binding structure of the antigen and antibody ELISA can be classified as three types namely direct, indirect, sandwich, or competitive(Figure 6)[34]. In the direct type of detection, the primary antibody labeled with the enzyme directly reacts with the antigen. Direct detection is not extensively used for detection but instead, they are used for immunohistochemical staining of

tissues and cells[35]. In the case of indirect detection, a secondary antibody is employed for detection as discussed in the above section. Incubation with pre-labelled secondary antibodies are done[35, 36]. The high specificity of the antibody-enzyme complex is important and is attained when the antibody is affinity-purified and the conjugation can preserve the antibody specificity and enzyme activity. The nonspecific signal due to cross-reactivity of the secondary antibody is possible and extra incubation steps are the drawbacks of this type. Increased sensitivity and the ability to use different visualization markers can be the primary advantages. Sandwich ELISA is the most commonly used technique. The analyte is bound between two antibodies, the capture and detection antibodies with a label. This technique is more sensitive and robust. In competitive technique, unlabeled antigen in the test sample competes with labeled antigen to bind to the antibodies. Unlabeled antigens reduce the ability of labeled antigens as they have already occupied the binding site. In this type the less the signal from the label produced, the more the unlabeled antigen in the test sample is present. The amount of antigen in the test sample is inversely associated with the amount of signal produced for detection.

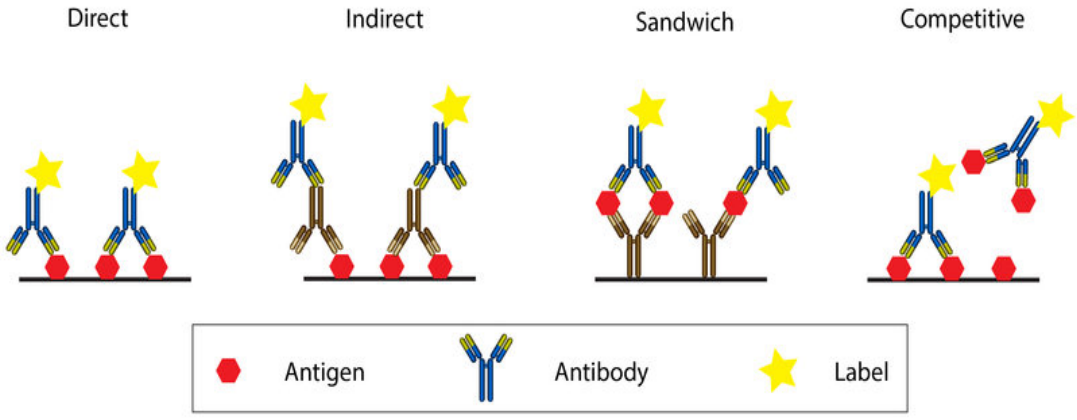

Figure 6: Illustration of direct, indirect, sandwich, and competitive ELISA[2].

2.3. Digital ELISA

Compared to the conventional ELISA discussed above which are done on tubes or microtiter plates, digital ELISA is done in a much smaller scale. A high-density array of micrometer-sized containers are employed to partition the reaction solution and perform the same assay. This allows the compartments to be filled with either 0 or 1 target molecules. In contrast to conventional ELISA where quantification of the absolute intensity of the microtiter wells, only the microwells showing positive signals are counted. Due to the unique binary property of the technique, it is called a digital assay. This technique possesses several advantages such as high sensitivity and resolution, minimal requirement of sample and reagent, lower cost, faster analysis times and provides the ability to study single molecules. In conventional ELISA techniques, an enormous amount of analyte molecules and enzyme labels are required to generate the signal that can be detected by plate readers. This pushes the sensitivity of the technique to the picomolar range(10^{-12}M) and above. However, the digital assay is based on either presence or absence of signal making the theoretical limit of detection down to the attomolar range(10^{-18}M). In cases where early-stage detection of cancer is done in serum samples with biomarker proteins expressed in less than picomolar concentration, digital bioassays are highly expedient. The principle of the technique is the same as the sandwich ELISA. The target molecule is held in between capture antibody and detection antibody with a label.

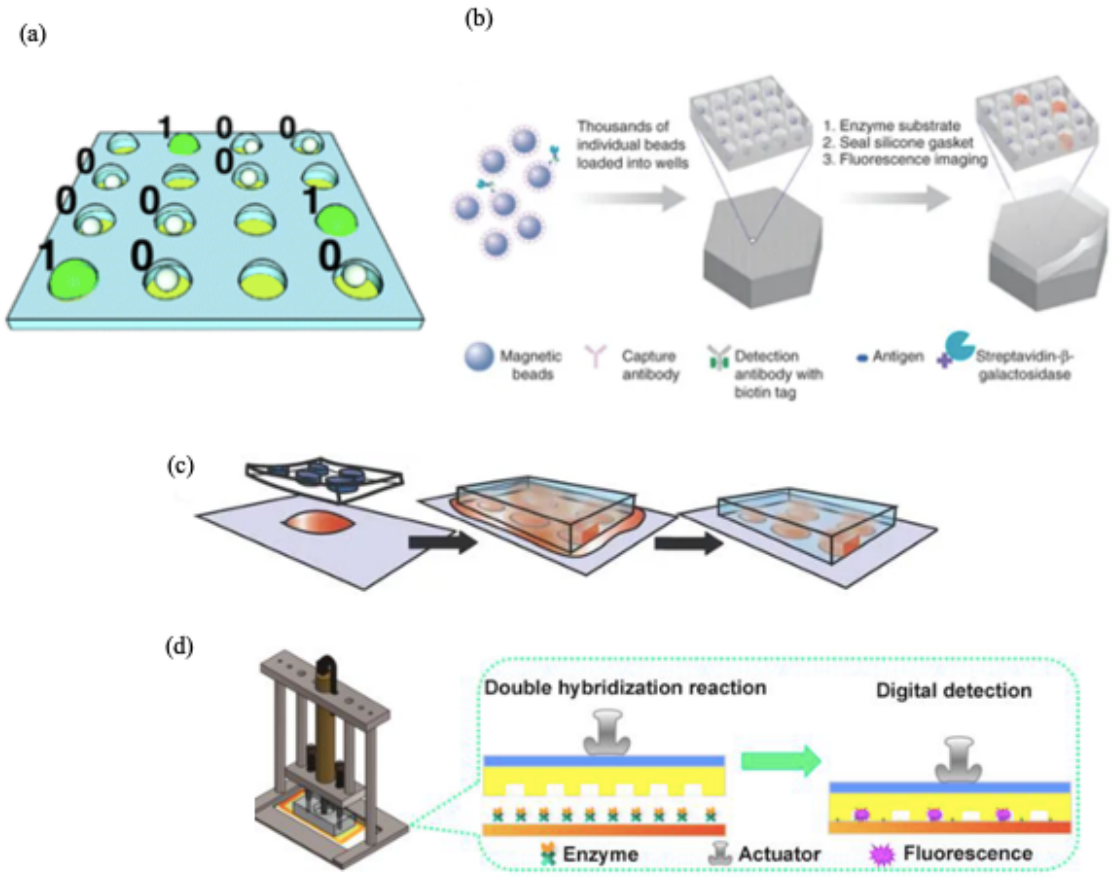

Figure 7: Different types of digital ELISA (a) Droplet array based digital ELISA[7], (b) Single molecule array technology in fiber optic cable[10], (c) Isolation of reagents into PDMS compartments for analysis[11], (d) Digital ELISA on captured targets on substrate[12].

Compartmentalization of such minute volume can be done by creating a femtoliter droplet array (Figure 7a). Polystyrene beads with 0 or 1 captured analyte molecules are introduced into the individual droplets for quantification[7]. These functional beads captured with target analyte molecules could also be loaded into femtoliter-sized microwells for detection by enzymatic fluorescence amplification. These microwells were fabricated in optical fiber bundles by chemical etching (Figure 7b)[10]. This technique is called as Single Molecule Array Technology (Simoa).

Beads conjugated with capture antibodies are mixed with the test analyte sample at a higher concentration than the analyte. Then these beads are individually loaded into microwells and sealed. The presence of analyte can be detected by the fluorescence produced by the enzyme labels

conjugated with the detection antibody that is bound to the target analyte after washing. However, this technique involves a complex experimental process as it uses oil to seal the microwells. Also, compartmentalization of the reagents can be directly done using a microwell array fabricated in PDMS[1, 11]. The reagent mix can be forced to compartmentalize into microwells by sealing (Figure 7c). But this technique cannot be done to study individual molecules as the distribution of reagent molecules will be inconsistent. The sandwich ELISA assay can be performed on a solid-state substrate like glass and the microwell array can be enclosed on to the glass to partition the bulk reagents into small compartments (Figure 7d). They used a manual actuator to seal the microwells in the PDMS chip, but as it is a manual one, there will be inconsistent sealing. The movement of the actuator is controlled manually with instructions to move for particular distances, making it an open-loop system. This increases the risk of breakage of the glass slide and also the time required to seal would be more as it is operated in manual mode. To overcome this drawback and to incorporate automation, a closed-loop actuation system was developed and is discussed in the section below and 4.4.

3. Automation in Digital Signal Acquisition and Image Analysis

3.1.Closed Loop System

A control system is a system in which the behavior of a device is controlled with the help of a control loop [37]. A process variable can be defined as a measured value of a particular process. Depending on the process variable, the control can be of two types namely open-loop and closed-loop control. In an open-loop system, the control action will be independent of the process variable, and the controller's action will not be influenced by the process variable. Whereas in a closed-loop control system the controller's action is dependent on the current and desired process variable. The desired value or setpoint is incorporated in a closed-loop system, based on which the process variable is controlled. This control is sustained with the help of a feedback loop. Open-loop systems do not employ feedback loops and are operated in a pre-defined manner. The closed-loop system has been incorporated in the actuation system used to seal the microwell array. It is discussed in detail in section 4.4. The main reason for this is to attain perfect sealing of microwells despite the variable chip thickness and to avoid breaking of glass slide in the chip. The closed-loop system is built with a force-sensitive resistor and an actuator where the process variable is force.

3.2.Force Sensitive Resistor (FSR)

Force-sensitive resistor (FSR) is a sensor that is capable of measuring the force applied to it (Figure 8a)[38]. In its active region the resistance of the sensor varies based on the load applied on it, and the force can be measured based on the varying voltage and current. The inner layer is made up of semiconductor material, and the and the outer layer is made up of a polymer named Mylar. It comprises of an active and a conducting film separated by a plastic spacer in between. When a load is applied, the particles on the active film touches the conductive film, reducing the resistance.

When there is no load applied on the sensor, it behaves like an open circuit with infinite resistance. And as the load applied increases the resistance decreases as shown in Figure 8b. The advantages of these types of sensors are that they are very sleek, low cost, and are shock resistant. The force range that the sensor is capable of measuring is from 0 to 20lb (0-100N)[3].

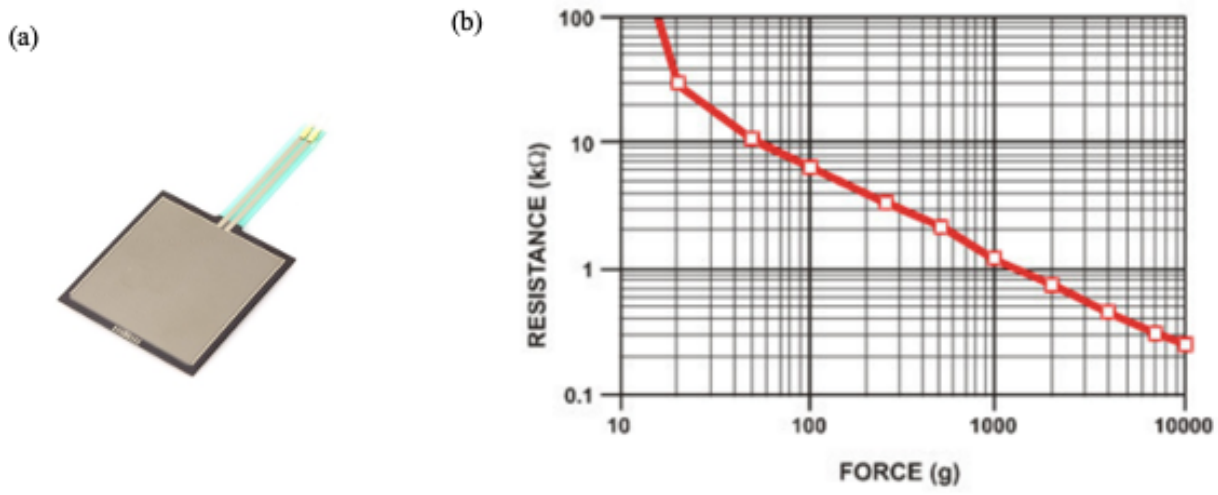

Figure 8: : Force Sensitive Resistor and its properties (a) A square FSR sensor and (b) Graph showing relationship between the applied force and resistance[3].

3.3. Image Processing

3.3.1. Hough Transform

Hough transform is used for extracting features image processing applications and video processing applications [39]. This can be used for detecting lines circles and eclipses. In the Hough transform, the accumulator spaces are first created. It has a cell for each of the pixels present in the image. In the beginning, all the cells' values are set to zero. The edge point in the image will be detected first. The equation of the circle, where a and b are the coordinates of the center and r is the radius of the circle Is used by the algorithm.

The edge pixels in the image are the ones with a high-intensity gradient in intensity that will come back to the background pixels [40, 41]. These foreground edge pixels are the candidate pixels. These pixels cast votes in an accumulator array. These candidate pixels consider themselves as the center pixel and then vote for all pixel coordinates that could possibly be on the circle for the given radius. Therefore, the peak values of the accumulator array correspond to the center of the circles. In MATLAB, both the techniques available uses only one two-dimensional accumulator array for the radii range. This increases the computational efficiency but reducing the computational load even when there is a large radius range. Since only candidate edge pixels of the high gradient are considered while counting votes, the speed is high, and memory consumption is low. The two-stage algorithm is based on computing the radial histograms. In other words, the radius is directly estimated from the calculated circle centers.

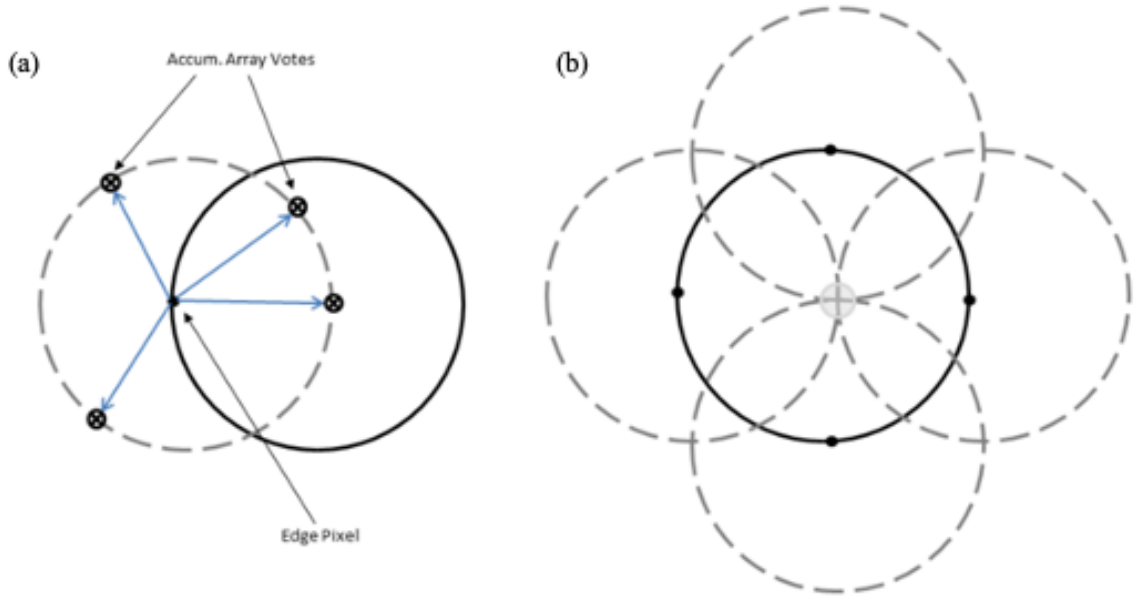

Figure 9: Representation of (a) an example of candidate pixel in an actual circle (solid) and accumulator array votes and (b) finding center of the circle[4].

3.3.2. Contrast Enhancement

Contrast enhancement is a technique in image analysis by which the intensity distribution is manipulated to cover a broader range [42]. This is done because when the pixels' values are highly varying it is quite easy to distinguish the features in an image than when the pixel distribution is highly narrow. The contrast enhancement applied to an image can be visually perceived through the histogram plot of the image. Histogram plots the pixel intensity distribution of an image. In other words, the histogram is the probability density function of the pixel intensities of an image. Consider an image with L gray levels. To plot a histogram, the number of pixels corresponding to each pixel intensity will be calculated. This will be then be plotted as a histogram as pixel value vs the number of occurrences. Before contrast enhancement, the image histogram is confined to a specific band of intensity. Once the enhancement is performed, the intensity band is focused on the intensity band of interest in the histogram plot.

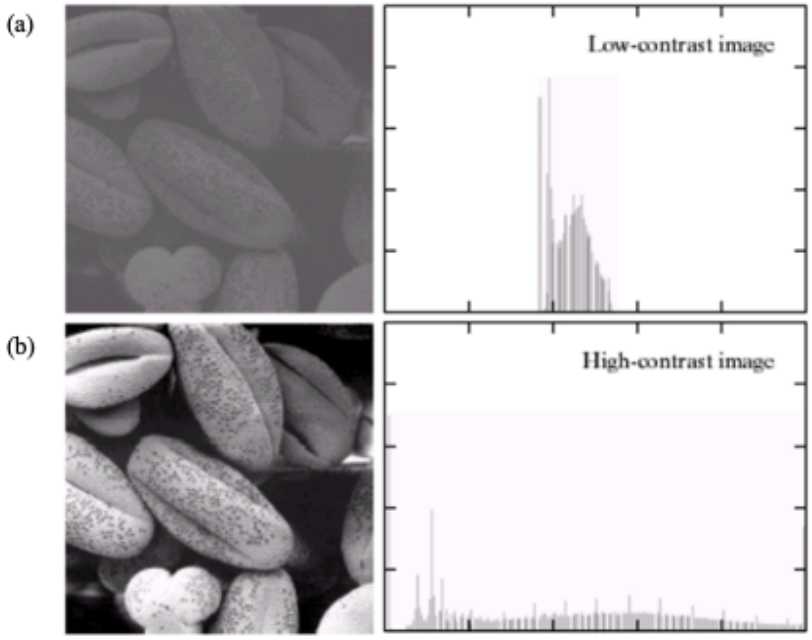

Figure 10: Representation of (a) low and (b) high contrast image.

4. Experimental Methods

4.1. Reagents and Materials

Monoclonal Anti-human CD81 (Ancell, 302-820) was used as a capture antibody for exosome, and antibody cocktail composed of biotinylated anti-CD63 (Biolegend, 353-018), and biotinylated anti-CD9 (Ancell, 156-030) was used as detection antibodies. Standard exosome isolated from COLO-1 cell culture media (Galen Laboratory Supplies, Middletown, CT) was used for analysis. Poly-L-lysine (PLL) solution (P8920), (3-Aminopropyle) triethoxysilane (APTES), glutaraldehyde, and Tween 20 (P9416) were purchased from Sigma-Aldrich. Phosphate-buffered saline (1× PBS, pH 7.4, Mediatech, Inc.), fluorescein di-β-D-galactopyranoside (Invitrogen), streptavidin β-galactosidase (SβG) conjugate (Invitrogen), SU-8 (MicroChem), polydimethylsiloxane (PDMS, Dow Corning), were employed as received. Bovine Serum Albumin (Sigma Aldrich) was used for blocking in blocking buffers. SβG and FDG were dissolved in PBS working buffer (PBSW) which comprises of 5% BSA and 2mM $Mgcl_2$ (Fluka Analytical) in PBS.

4.2. Design and Microfabrication of Microfluidic Chip

The design of the microfluidic chip containing several chambers, channels, and inlet and outlet ports was designed using AutoCAD (Figure 11). The chambers involve the lysis chamber and the detection chamber. The lysis chamber was designed to lyse the enriched EVs with minimal dilution and to pump it to the detection chamber. It was designed for an additional application to monitor EV lysate for potential cancer biomarkers and it is discussed in section 6.2.2. In this study, as the goal was to detect individual EVs, the lysis chamber was not used in the methods. The ports perpendicular to the detection chambers was used as inlets, the ports to the right of the detection

chamber were used as outlets and lysis chambers were allowed to permanently bond to the glass slide, making the left half of the chip unused. The detection chamber contains the microwell array for obtaining the digital signal. The molds for the fabrication of the chips were prepared using silicon (Si) wafers and SU-8 using the standard photolithography technique. And the PDMS chips were fabricated using the soft-lithography technique. The silicon mold for the pneumatic layer was fabricated with SU-8 2025 photoresist with a final thickness of 40µm by following the fabrication instructions from the manufacturer. The fluidic layer mold was prepared by two-step photolithography. Initially, 20µm thick features for the fluidic channels and ports except the microarray area were patterned using SU-8 2025 photoresist. It was then followed by fabricating another 10µm microarray features using SU-8 2010 photoresist. After post-exposure baking at 95ºC for 5 min, the pattern was developed for 5 minutes and hard-baked at 200ºC for 2 hours. Before fabricating the PDMS chips using the mold, overnight treatment with trimethylchlorosilane by gas-phase silanization under vacuum was done.

PDMS chips were cast from the Si molds that were fabricated. PDMS mixture at a ratio of 12:1 (base material: curing agent) was thoroughly mixed, degassed for about 20 min and poured over the corresponding mold. It was then cured in the oven at 70ºC for 2 h, during when the PDMS solidifies. The PDMS slab with the replica of the pneumatic layer was cut and peeled off from the mold and access holes were punched for pneumatic valve connections. Meanwhile, for the fluidic layer, 7g PDMS mixture at a ratio of 10:1 (base material: curing agent) was spin-coated over the mold at 800rpms for 30 s and cured in the oven at 70ºC for 2 h. To prepare the double layer chip the pneumatic layer and the fluidic layer were treated with UV for 5 min and manually aligned with the help of a stereomicroscope. For the permanent bonding of the two layers, the chip was

baked at 80ºC overnight. The assembly was then removed from the mold and access holes were punched using a biopsy punch for fluid inlets and outlets.

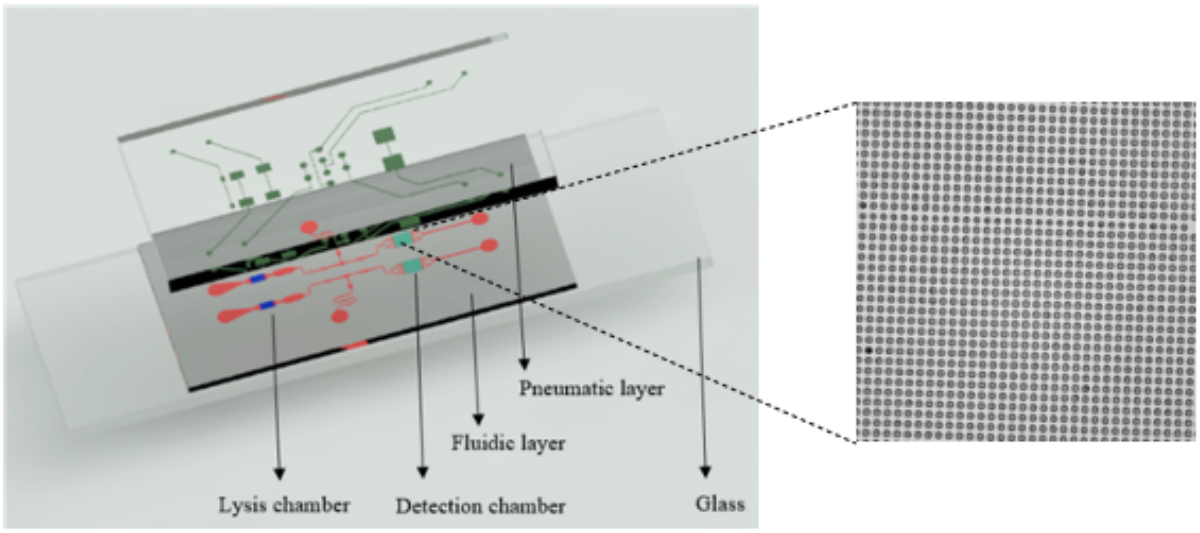

Figure 11: Schematic illustration of the design of a three-layer PDMS/Glass chip that has an eight-valve system, lysis and detection chambers

4.3. Microfluidic Pumping and Inter-channel Leakage Test

The pneumatic valves and the chambers were pneumatically actuated using a homemade solenoid controller previously built by our lab[43]. It is interfaced with a computer using a LabVIEW program. Integrated pneumatic pumps and valves allow real-time monitoring and control of the flow. A five-step stop flow pumping method was incorporated to pump the reagents[44]. It creates a peristaltic motion using by actuating the valves sequentially. The closing of the valve is achieved by applying pressure and the opening of the valve is achieved by applying a vacuum. 30kPa was the closing pressure used for all the pumping except for washing and the vacuum at -80kPa. During washing the pneumatic valve above the detection chamber was also flipped but only halfway through by reducing the closing pressure to 15kPa. This additional step during washing is done to increase the efficiency of washing and to evade molecules getting non-specifically bound to PDMS

in microwell array. Food dyes were used to visualize the motion of fluids in the chip during pumping and the flow rate was optimized accordingly. 10µl of water colored with food dye was injected to the inlet and it was pumped with different delay timings for each step and the time taken to pump the entire fluid was measured. The timing delay of each step was changed to get the required flow rate and it was optimized for different steps of the assay.

To check if there is any leakage within its two separate channels, food dye was pumped in one channel, and water without any dye was pumped in another channel. This test was done after bonding the PDMS chip to the glass slide, for about 1hr. This is an important test to avoid any false positives during the experiment.

4.4. Building Closed-loop Actuator System

The actuator setup was designed in such a way that it would fit onto the stage of the microscope (Figure 12). The integrated system comprises the actuator, FSR sensor, and Arduino microcontroller. A custom-built stage was designed and fabricated in Aluminum to hold the actuator and would also fit onto the stage of the microscope. FSR was fixed at the bottom right of the base of that holder using a double-sided tape and a paper along with a double side tape with almost the same thickness was placed on the other side. It is to even out the height when a chip with a glass slide is placed.

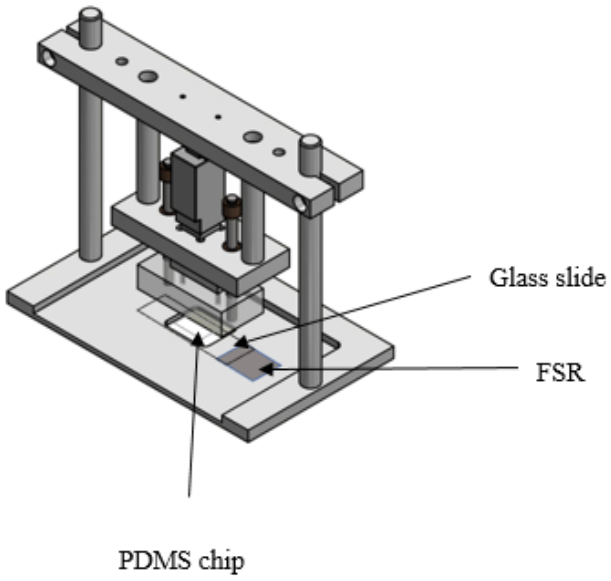

Figure 12: Design of the actuator setup with FSR

Actuator presses the detection chamber of the microfluidic device for sealing of microwells, the force sensor (FSR) senses the force applied on it and sends the force value to the Arduino microcontroller as negative feedback (Figure 13a). The microcontroller controls the position of the actuator based on the sensed force value. If the value is less than the setpoint or the threshold mentioned in the code, the microcontroller commands the actuator to move further downwards (Figure 13b). Initially, until the actuator arm touches the chip, the force values detected by the sensor would be 0 and thus the actuator arm would keep moving towards the chip. Once the actuator arm starts coming in contact with the chip the force value sensed by the sensor increases. A particular range of force value needs to be mentioned in the code so that the microcontroller can make the actuator stop. If the sensed force is greater than that particular range of setpoint values, the algorithm is programmed in such a way that the actuator can retract back. This additional condition in the program is to avoid breakage of the chip if the exerted force increases beyond the specified setpoint range.

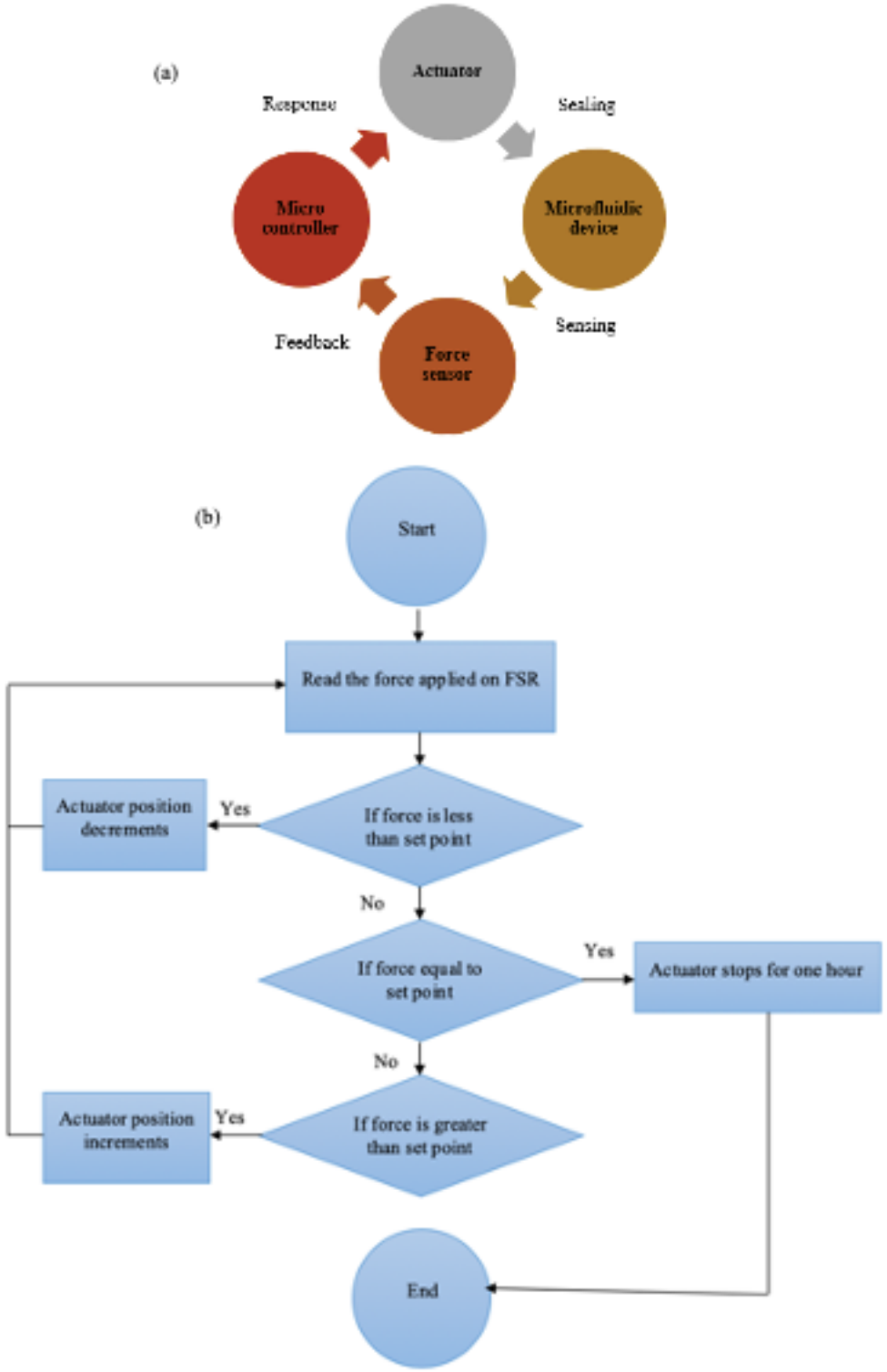

Figure 13: Schematic explanation of (a) Workflow of the closed loop actuation system. (b) Algorithm of the Arduino code.

4.5. Connection of Closed-loop Actuator System

The components involved in the circuit are Arduino UNO, FSR sensor, 10kΩ resistor, 12V supply adapter, Actuonix linear actuator, and LAC board that comes with the actuator. One end of the FSR was connected to the 5V pin of the Arduino and the other end of the sensor was connected to a pull-down resistor and then grounded. The resistor and FSR's connecting point was also connected to an analog pin A0 of Arduino to read the values from the FSR (Figure 14). The actuator had five wires and it was directly plugged to the LAC board which was designed for it. The LAC board was intended to control the actuator without any external sources needed. But as in our case, there is FSR involved, the controlling factor of both FSR and actuator was designed to be Arduino. A 12V power supply from an adapter was connected to the LAC board. The LAC board was commonly grounded with the Arduino and the output from the RC pin which is used to control the actuator position was connected to pin 9 of Arduino.

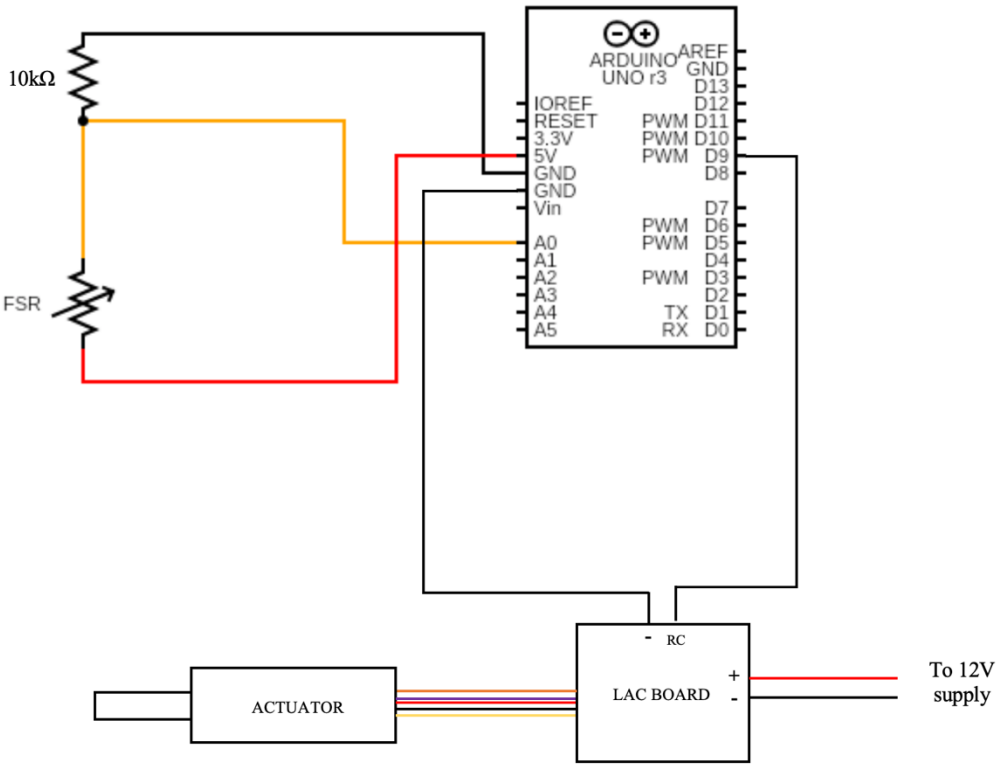

Figure 14: Circuit connection of the closed loop actuation system

4.6. Determining Set Point Force Range for Actuator System

The range of the setpoint is mentioned as analog values in the program. The reason is that the FSR gives corresponding analog values from 0 to 1023 (0-5v) indicating voltage based on the load applied on it. For the ease of optimization and to eliminate any errors during the conversion, the analog values were used in the Arduino code. The range starting from 700 with an increment of 30 were tested to determine at which range of values the chip would break. These analog values will be then converted into force (N) values by the code and be displayed in the serial monitor of Arduino software.

4.7. Photobleaching Experiment

To ensure the sealing performance of the actuator, 100µM fluorescein dye diluted in water was made to flow into the microwell area via the channels. The actuator was made to seal the microwells and light source was focused on the center of the microwell array and allowed to photobleach. Images were taken every 20 min and the entire test was conducted for up to 1hr. Percolation of the dye from the un-photobleached area to the photobleached spot will be inspected.

4.8. Free Enzyme Assay

In this assay, the reporter enzyme SßG (10ng/ml) and the substrate FDG at 500µM concentration will be premixed in the working buffer PBSW and immediately injected into the microwell area of the chip. The actuator will be immediately activated to seal the microwells in the detection chamber (Figure 15). This experiment is to further test the ability of the actuator to seal microwells and to determine an optimal sealing time for the assay. Images were taken at 10 and 20 minutes after the sealing at 5% light intensity and 6000ms exposure.

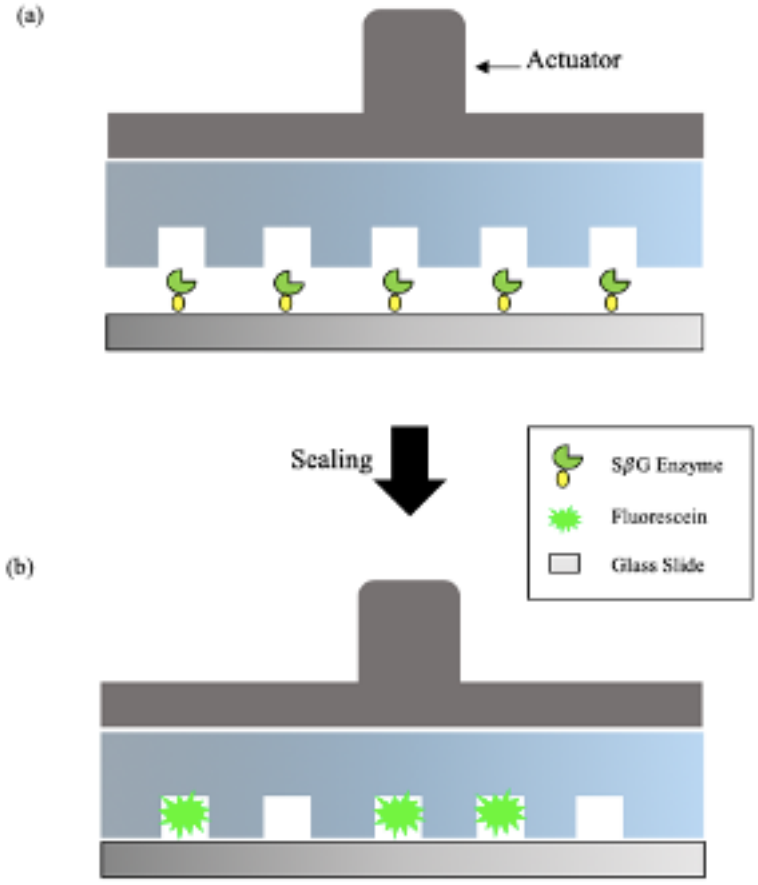

Figure 15: Schematics explaining digital signal acquisition (a) Before sealing the microwells onto the glass slide, (b) After sealing to produce digital signal.

4.9. Comparison of PLL and APTES for Surface Patterning

Initially, the surface silanol groups of the glass slides were activated by immersing them in piranha solution (3:1 concentrated sulfuric acid: hydrogen peroxide) for at least 30 min. For APTES surface modification, the glass slides were immersed into 2% APTES in Toluene after cleaning with deionized water and were allowed to react for 2 hours. The amine group modified glass was removed from the solution and rinsed with ethanol, airdried with N_2 gun, and baked at 110ºC for 2 hours to crosslink the monolayer. Then the glass slide was shaken in 2.5% (v/v) glutaraldehyde in PBS for introducing aldehyde functionality. For modifying glass slides with poly-l-lysine, the

protocol from the manufacturer with few modifications was followed. The freshly cleaned glass slide after piranha treatment was immersed in a 0.01% PLL solution in water and incubated for 5 minutes at room temperature. Then the excess PLL was drained 3 times with deionized water and was cured in an oven at 60ºC for 1 hr. Specific areas of the glass slide were patterned with anti-human CD-81 capture antibodies (100µg/ml) in PBS with the help of the patterning chip. The same protocol mentioned below in the digital ELISA section was implemented to compare the surface patterning.

4.10. Quantification of Total Extracellular Vesicles present using Digital ELISA

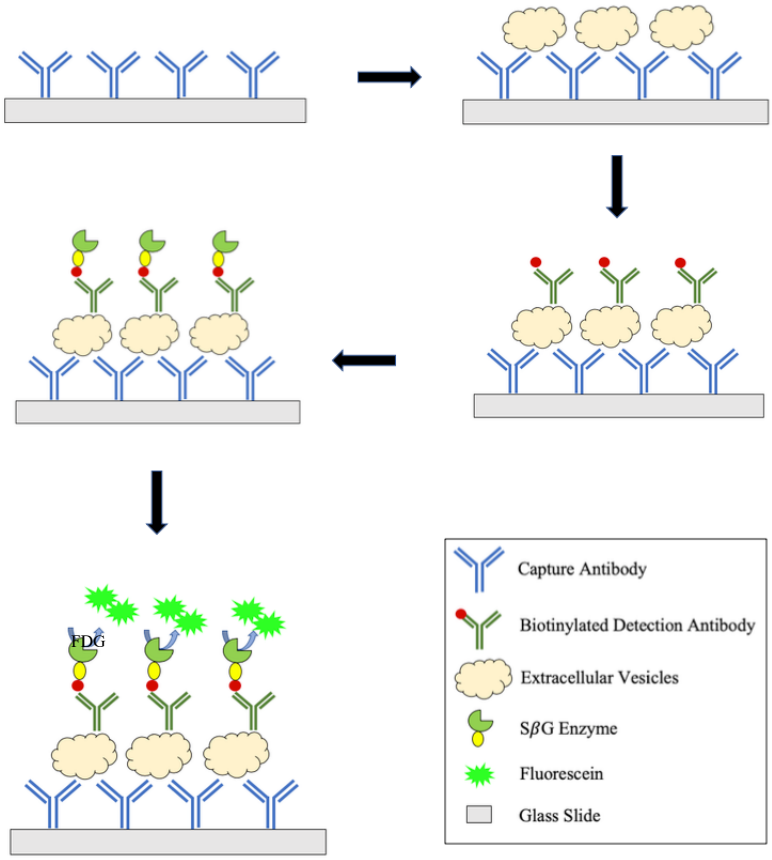

Figure 16: Schematic of the workflow of Digital ELISA protocol. EVs were captured using immobilized capture Abs. Then using the biotin labelled detection antibody and the reporter enzymes SßG they were digitally detected.

Glass slides were immobilized with PLL as mentioned in the surface patterning section. Capture antibodies at 100µg/ml concentration in PBS were immobilized in specific areas of the glass slide with the help of a patterning chip (Figure 16). The incubation was done overnight in 4ºC. The microfluidic chip was treated with UV for 5 minutes and was aligned onto the glass slide with immobilized capture antibodies. Markings were done on the back of the glass slide, right below the patterning chip for reference. Then the UV treated PDMS chip was aligned such that the detection chamber is on top of the patterned area. Immediately after bonding the PDMS chip to the glass slide, 5% BSA in PBS was made to flow through the channels for blocking, and the pumping was done for 1h. After 1h the channels were rinsed with PBST (1%BSA 0.005% Tween20 in PBS) for 5 minutes. Then 15µl of analyte which is standard exosomes (in 0.1% BSA PBST) in this case were injected at various concentrations. After 2 hours of stop flow pumping of the analyte, the channels were washed with 1% BSA in PBS. Then a cocktail of biotinylated detection antibodies (Anti CD-9 and CD-63) was made to flow at an individual concentration of 100ng/ml in 1% BSA were mixed and pumped through the chambers for 1h. After an hour, excess detection antibodies were rinsed with PBST containing 2mM Mg^{2+} for 15 minutes. Additional rinsing of the inlets was also done for 3 times with a pipette, before rinsing the chambers of the chips to avoid any non-specific false-positive signals. Followed by the washing, 15µl of streptavidin-conjugated β-galactosidase (SβG, 5 ng/mL) in PBSW was introduced to the chip. After about 30 min, the assay channel was thoroughly washed with PBST containing 2mM Mg2+ for 15 minutes and then filled with fluorescein di-β-D-galactopyranoside (FDG, 500µM). The closed-loop actuator was activated to press down the detection chamber of the chip and seal the microwells. Incubation was done for the optimized time and images were taken with a fluorescent microscope at 470nm wavelength, 5% intensity, and 6000ms exposure time.

4.11. Automated Analysis of Digital Microwell Images using an Image Processing Algorithm

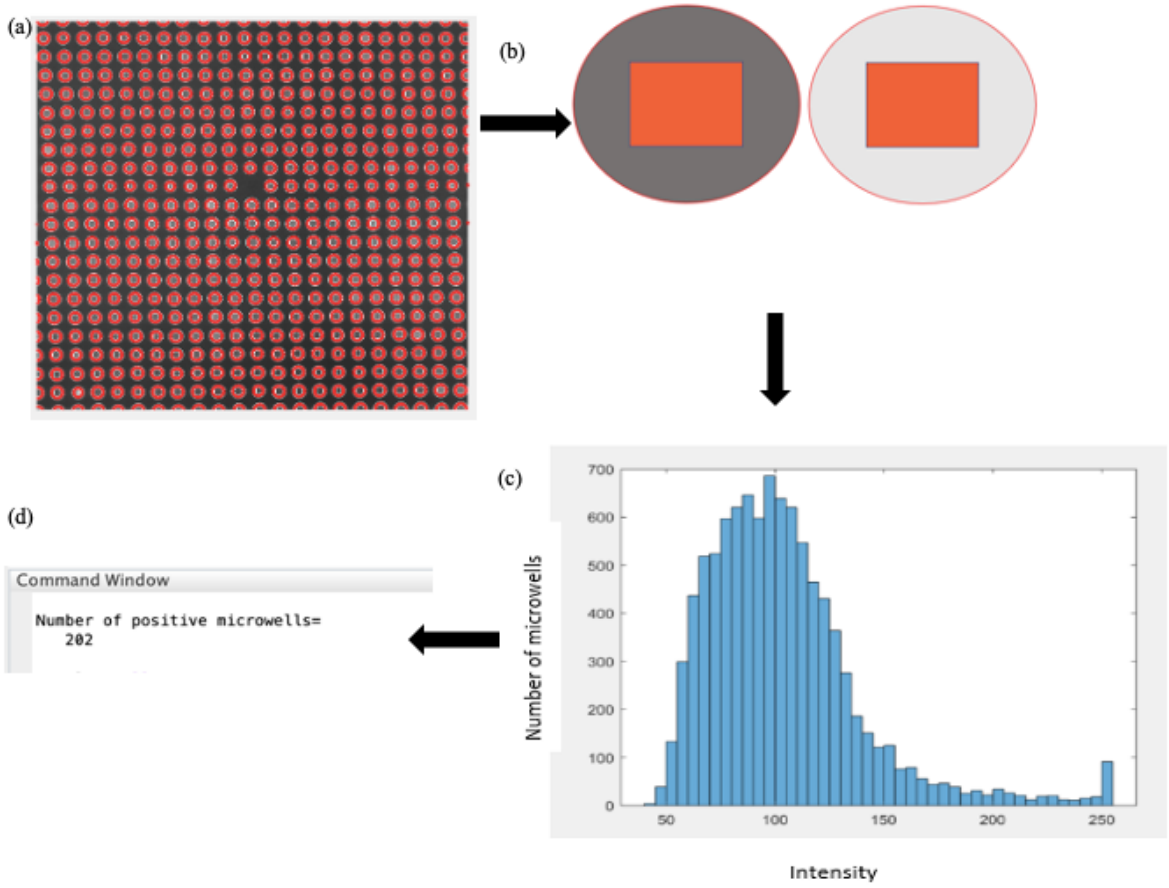

Figure 17: Workflow of the automated image analysis (a) Microwells detected by the algorithm. (b) Illustration of a negative (left) and a positive (right) microwells, showing the area (red square) considered for calculating the average intensity. (c) Histogram showing number of microwells at each intensity value. (d) Screenshot of MATLAB command window showing the output of number of positive microwells.

Initially, a loop was created to read individual image segments of the microwell array. The Nikon Eclipse Ti2 microscope used in our lab is capable of acquiring large images by scanning. It can capture sixteen individual images and stitch them together giving an overall image of the microwell array. The loop was designed to consider each image and analyze them. While analyzing the final stitched image, the detection sensitivity of the algorithm was trimmed down. Therefore, to maintain the sensitivity, individual images were considered for the analysis. The raw images were contrast-enhanced using the Image J software and saved in a separate folder. These

images were used to improve the sensitivity of the detection of circular microwells. But they were not used for any analysis.

The following processing and analysis were done on each image segment. Initially, a contrast-enhanced image was used to detect the circles. As a one-time setup, using the MATLAB function imdistline, the pixel value radii of fifteen microwells was measured. The average was around 10 pixels. Imfindcircles function was used to detect the circles and extract the center and radii data of each circle in that individual image (Figure 17a). It uses the Hough transform to detect the circles and get the center and radius data. Radii range of 9 to 11 was assigned as the radius range for detection in imfindcircles function. The object polarity was set to bright in the imfindcircles command, as the circles were detected in a dark background. Two-stage was the method used to detect the circles and it was specified in the function. Two-stage is preferred over phase coding because it can detect circles at low sensitivity levels[41]. This yielded the coordinates of the center and the value of the radius of each circle. Using the center coordinates, the circles were drawn and displayed on the unprocessed raw images. All further analyses will be performed only on raw images. The circles were drawn using the viscircles command in MATLAB. This function is just used to visualize the circles around the perimeter of microwells. Using the center and radii data this function can draw circles in an image. Then a sub-loop was created to find an average pixel intensity for each microwell. 36 pixels around the center were considered and an average intensity was obtained for all the microwells (Figure 17b). Finally, to count the number of positive microwells, the average intensity value of each microwell was compared to a predefined threshold intensity to consider it as positive. Another separate subloop was created to calculate the number. The predefined threshold value was set as 3 standard deviations above the mean background and it was 3200 in the 16-bit image (0-black and 65535-white). The background was

the microwells with only FDG autofluorescence. The value of the number of positive microwells was stored in a variable and the same process was repeated with the next image. The positive well count was added to the previous counter value and the loop continues to all the remaining images. In the end, a final count value of the number of positive microwells was made to be displayed in the command window of MATLAB (Figure 17d). The MATLAB code of this algorithm is included in Appendix 7.2. Another modified version of this algorithm to detect and analyze shapes other than circles is also discussed in Appendix 7.3.

4.12. Algorithm Testing for Accuracy and Precision of Microwell Detection

The accuracy of the algorithm to detect the circles was evaluated with a microwell array image. As a negative control blank image with just PDMS and no microwell array was considered. This is done to verify that the algorithm does not detect any false positives. 16 negative control images were used to test the algorithm to see if it detects any circles even though there were not any. 16 microwell array images were used to test the accuracy of circle detection. The total number of microwells counted by the algorithm was compared with manual counting to calculate the accuracy of detection. To test the precision, each image will be run three times in the algorithm. The algorithm is expected to output the same results every time for an image.

5. Results and Discussion

5.1. Design and Microfabrication of Microfluidic Chip

The master mold was fabricated using the photolithography technique as described in section 4.2. The pneumatic or control layer master mold includes features for the pneumatic valves, pneumatic channels, and inlets for pneumatic control tubing (Figure 18b). Whereas, the fluidic layer master mold contains features for the fluidic channels, chambers, and inlets and outlets for samples (Figure 18a). Patterns for capture antibody patterning chip were fabricated along with the pneumatic master mold. The physical features in the master mold after microfabrication was verified with the light microscope to ensure the pattern is as designed. The final PDMS microfluidic chip was fabricated by casting two layers with the Si master mold and aligning it (Figure 18c). The alignment was accomplished using a stereomicroscope after exposing the pneumatic and fluidic layer to UV for 5 min. After allowing it to permanently bond by curing it at 80ºC overnight, the bonding was manually checked to see if the layers stay intact. The casted features in PDMS chips such as the chambers, channels, and especially the microwell array was checked with a light microscope for any defects.

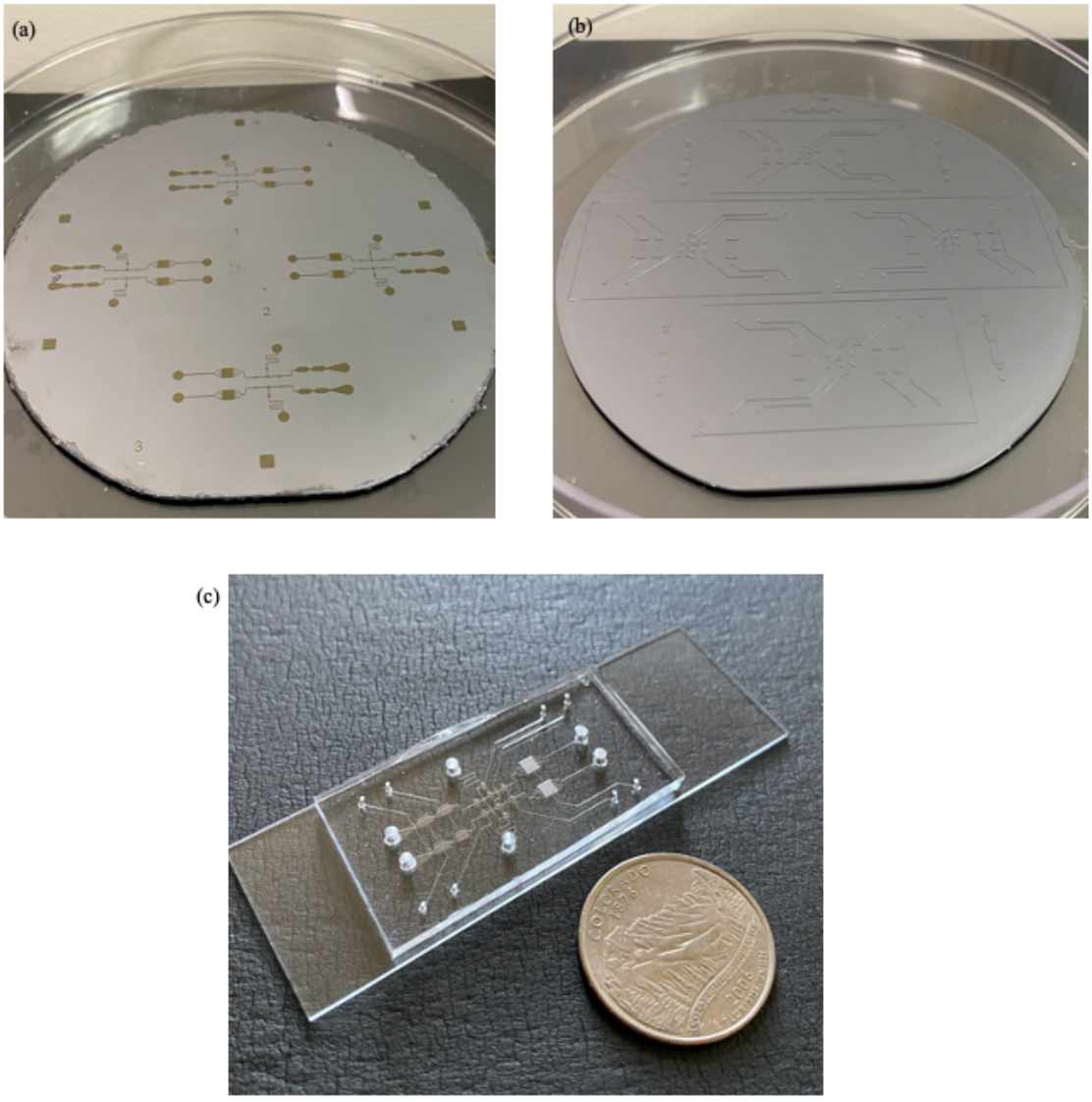

Figure 18: Final microfabricated (a) master wafer for fluidic layer, (b) master wafer for pneumatic layer, (c) PDMS chip after aligning fluidic layer and pneumatic layer and then bonded to glass slide.

5.2. Microfluidic Pumping and Inter-channel Leakage Test

A five-step stop flow pumping method was utilized to pump the reagents. 30kPa was the closing pressure used for all the pumping except for washing and the vacuum at -80kPa. Food dye was used to visualize the fluid motion inside the microfluidic chip. Delay in milliseconds was optimized based on the required flow rate. The final delay values are shown in Table 1 below for corresponding flowrates and reagents of the assay.

Table 1: Delay set to achieve specific flow rates for various reagents involved in the assay.

Delay (ms) for steps 1-5	**Flow rate (µl/min)**	**Pumping reagent in assay**
500, 500, 500, 500, 3200	0.5	Blocking buffer
500, 500, 500, 500, 17200	0.125	Exosome sample
500, 500, 500, 500, 500	1	Washing buffer
1000, 1000, 1000, 1000, 1400	0.5	SßG

The leakage test was performed as discussed in section 4.3 and then outlets of channels 1 and 2 were visually inspected to see any inter-channel leakage between the two channels. The water in channel 2 would have been slightly colored if there was any inter-channel leakage, but no leakage was observed (Figure 19). The experiment was repeated for 5 different trials with different freshly prepared chips.

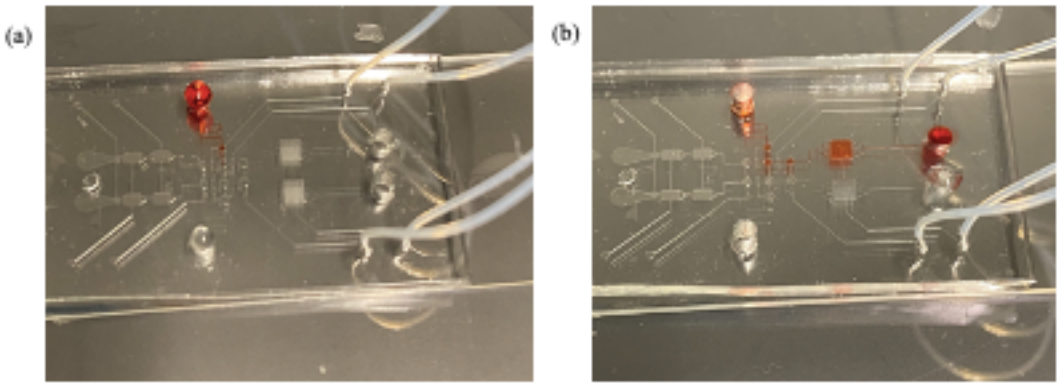

Figure 19: Inter-channel (a) Setup showing food dye and water in two inlets to test inter channel leakage. (b) Final image taken after the test showing no inter-channel leakage.

5.3. Building Closed-loop Actuator System

The final closed-loop system with the actuator, Arduino, and FSR was set up as discussed in section 4.4 and it looks as shown in Figure 20. The connection of all the components was done as per the circuit diagram mentioned earlier. The actuator started to move downwards as soon as the Arduino was connected to the computer. The FSR did not sense any load on it initially and the load values started to increase only when the actuator arm started to get in contact with the PSMS chip. The actuator stopped at the setpoint threshold values and sometimes it had to retract back when the load applied increased the setpoint and then stop at the desired force.

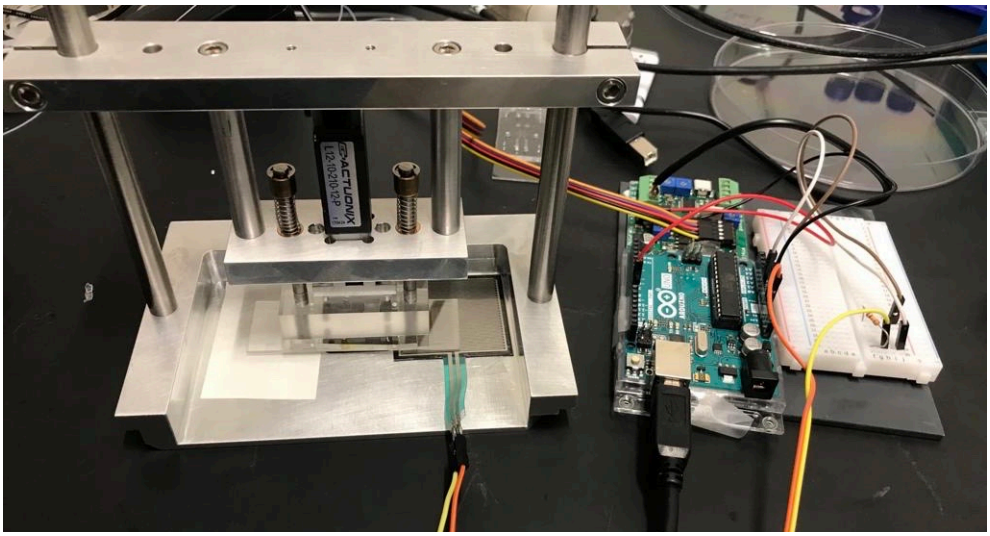

Figure 20: Final connected closed loop actuation system with actuator, Arduino microcontroller, and FSR.

5.4. Set Point Force Range for Actuator System

By testing with different analog voltage value ranges as the set point which represents the load on the actuator, the breaking point was determined. The corresponding force values in N was obtained from the serial monitor of Arduino and plotted against the probability of the chip not breaking (Figure 21). At lower forces, the chip did not break making the probability of non-breakage. But when the setpoint was assigned as values above 13N the chip could not withstand that force and the chip kept breaking. In the Arduino code, the setpoint value was defined as the force value equivalent to 12N. I kept the threshold slightly lower than the exact breaking point to avoid any unpredictable breakage. Even though the Arduino code was written to retract the actuator at force values beyond the set point, sometimes there might be a small-time delay in sensing and reacting to the actuator. To prevent any breakage due to this delay, the setpoint was set slightly less than the exact breaking point.

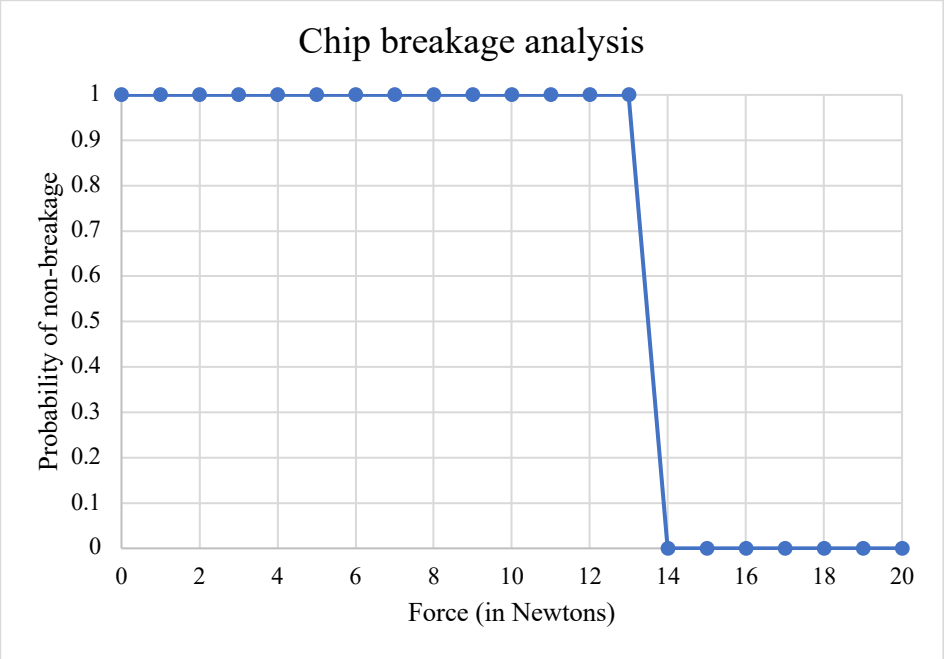

Figure 21: Graph showing the probability of breakage vs the force sensed on the FSR to determine the breaking threshold.

5.5. Photobleaching Experiment

The photobleaching test was done with 100μM fluorescein dye diluted in water. The primary goal of this experiment was to test for percolation of the dye from the unphotobleached area to the photobleached spot. The phenomenon where fluorescence intensity from the excited fluorophore gets reduced when continuously irradiated with light is called photobleaching. But if diffusion of unphotobleached dye occurs continuously to the photobleached area due to improper sealing, there would not be an absolutely dark circle seen in the focus spot. But fortunately, as shown in Figure 22 there was no diffusion of dye from the unbleached area to the photobleached area. This indicates that the sealing performance of the closed-loop actuator is sufficient enough to seal and confine fluid in individual microwells.

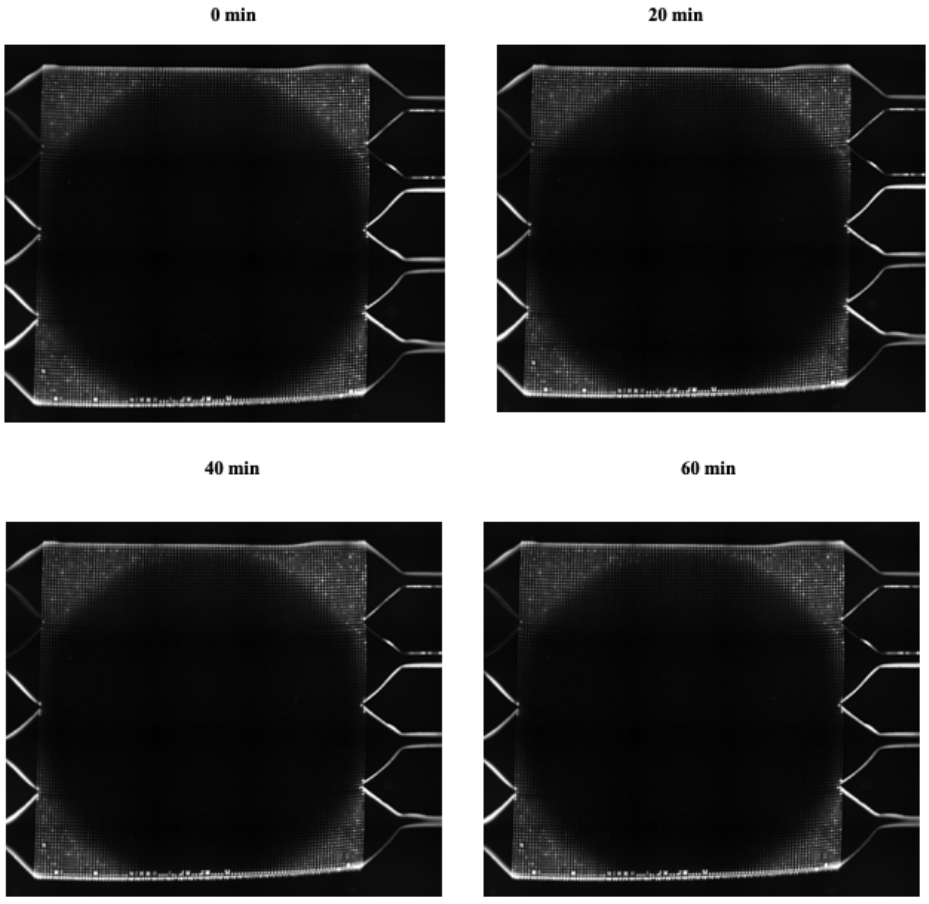

Figure 22: Images taken at 20-minute interval to test for any diffusion of dye into the photobleached area.

5.6. Free Enzyme Assay

The goal of this assay was to further confirm the sealing ability of the closed-loop actuator, verify the fluorescence produced by reporter enzyme SßG and the substrate FDG, and to determine the optimal sealing time for the final assay. By visually comparing the images taken after 10 min and 20 min, it can be concluded that 10 min is the optimal sealing time. For 20 min sealed incubation as shown in Figure 23b, diffusion of fluorescein produced due to the enzymatic fluorescence amplification reaction between SßG and FDG can be seen. Any time greater than 20 would have been incongruous because the spread due to diffusion would be much worse. And as the continuous fluorescence is produced in only microwells with SßG and not in the ones without SßG, it can be ensured that the enzymatic amplification reaction is working.

(a)

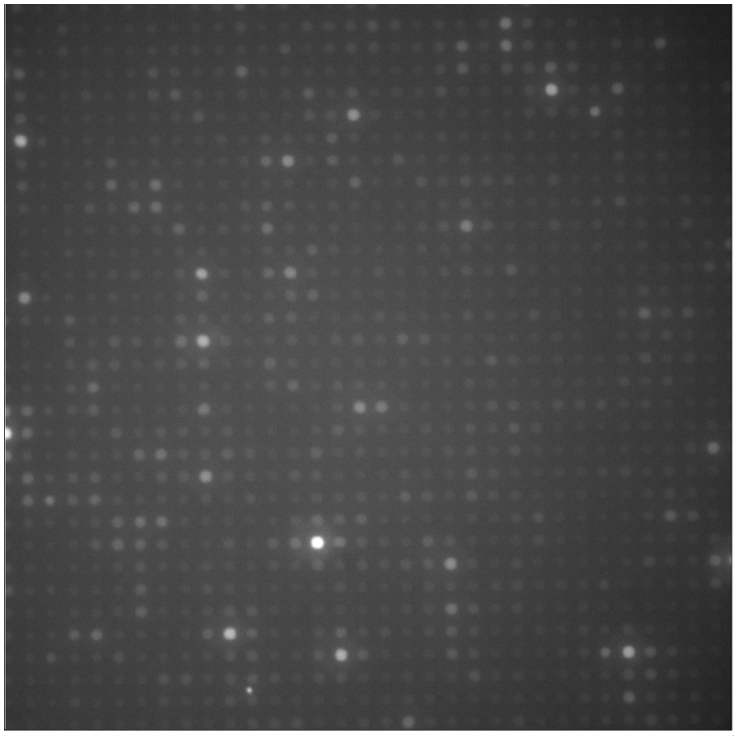

(b)

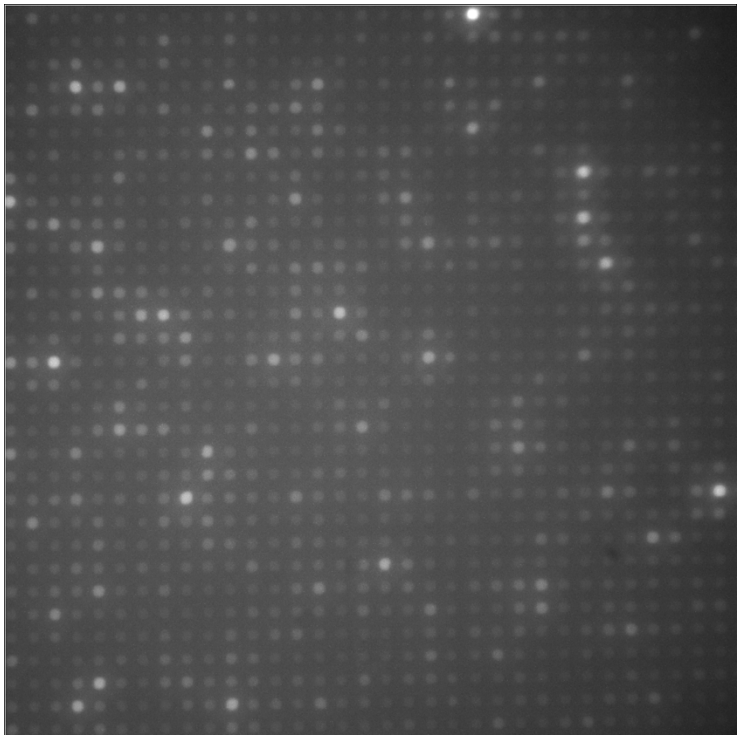

Figure 23: Digital microwell resultant image taken after (a) 10 min and (b) 20 min.

5.7. Efficiency and Precision of MATLAB Algorithm for Microwell Detection

Precision was tested by running the algorithm three times for each image. As shown in Figure 25 below, there are no error bars for each data point because it gave the same result for every rerun. This gives us a 100% precision, as the values do not change for a particular image considered in the algorithm. The accuracy for eliminating false positives was 100% as there were no circles detected in a blank image without microwells (Figure 24). This is depicted as a green line in Figure 25 shown below. Whereas the accuracy for detecting the circles in a microwell array image was 99.4%. The average number of detected microwells in a microarray image was divided by the theoretical total number of microwells present which is 10195. Sometimes the algorithm cannot detect few microwells in the corners of the microarray if they are slightly distorted while sealing. Or if they are too weak to be seen in the image even after contrast enhancement, they might go undetected. The accuracy is dependent on the quality of the image taken.

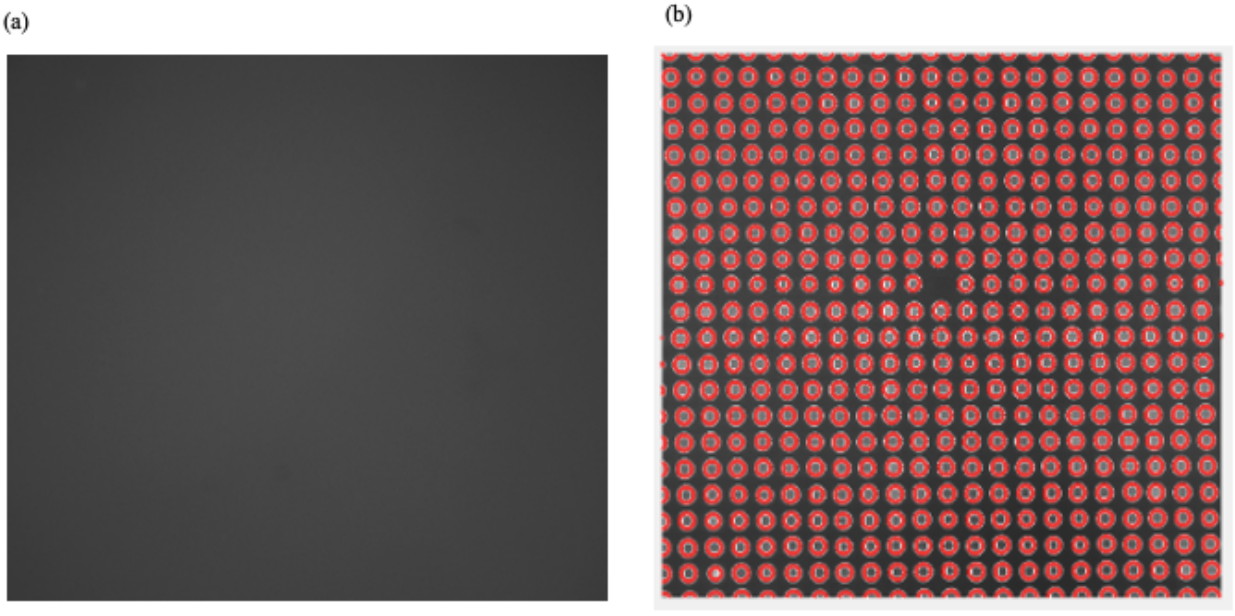

Figure 24: Accuracy determination of algorithm (a) Blank PDMS image used as negative control, (b) Microarray image showing detected microwells.

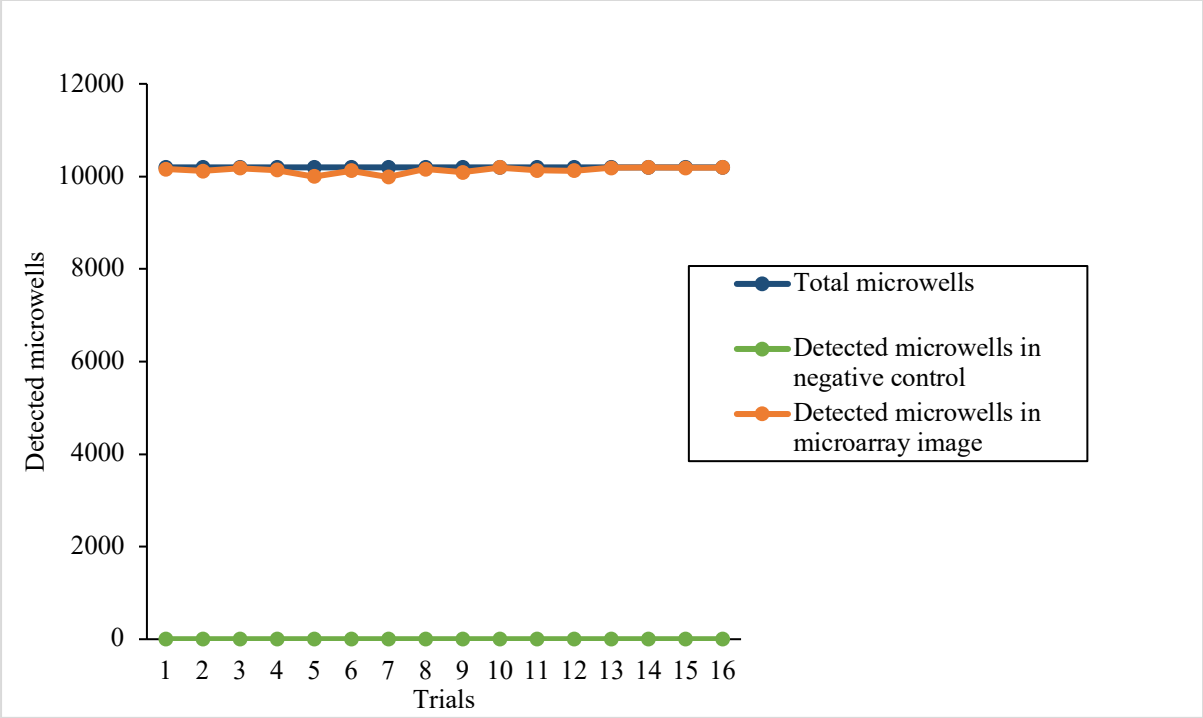

Figure 25: Resultant graph representing detected microwells in negative control, microarray, and total microwells present.

5.8. Comparison of PLL and APTES for Surface Patterning

An ideal surface modification technique to immobilize capture antibodies were determined in this experiment. Surface modification with APTES and glutaraldehyde was compared with PLL surface modification. The best surface modification technique was determined based on which has lower background or in other words the one with higher signal to noise ratio. As seen in Figure 26, APTES modified glass had elevated number of positive microwells for negative control. This indicates more non-specific binding of either detection antibodies or reporter enzyme. Whereas in chip with PLL modified glass the negative control is much lower compared to the APTES modified ones. The signal to noise ratio for APTES modified glass was 7.9 and for PLL modified glass it

was 80.6. As the signal to noise ratio is higher for PLL modified glass slides, it was chosen as the ideal surface modification technique for future experiments.

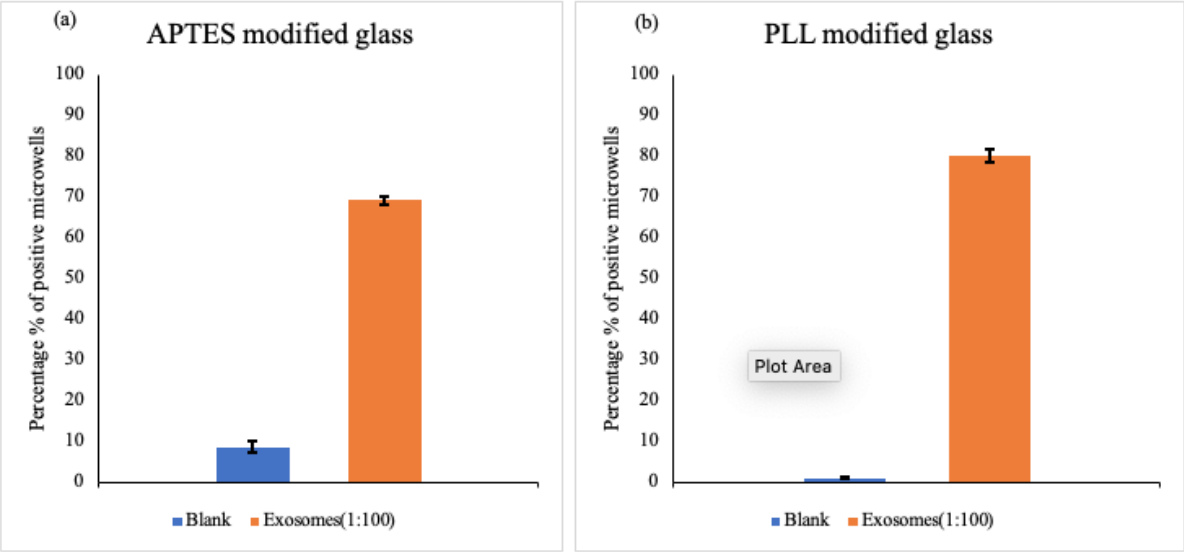

Figure 26: Bar plots showing the comparison of background and signal for detection of 10µg/ml of exosomes captured in (a) APTES and (b) PLL modified glass slide.

5.9. Quantification of Total Extracellular Vesicles Present using Digital ELISA

Exosomes were captured and detected using the digital ELISA technique by performing the protocol described in the experimental section. The stock solution concentration of the exosome standard was 1mg/ml ($9x10^{11}$ particles/ml). It was serially diluted 10, 100, 1000, and 10,000 times and was used in the assay to detect them on the chip. Anti CD81 was used as capture antibodies and anti CD9 and CD63 were used as detection antibodies to detect the exosomes. The images taken by the microscope were background corrected and were inputted to the MATLAB algorithm to quantify the microwells. Individual microscopic images and their corresponding outputs in the MATLAB command window is shown in Figure 27.

The concentration of exosomes in µg/ml as the logarithmic function was plotted against the logarithmic function of the percentage of positive microwells. The exosome quantitative detection was detected over a range of 10,000 times diluted exosome standard (100ng/ml, $9x10^{7}$

particles/ml) which had an average of 16.1% of microwells, to 10 times diluted exosome standard (100µg/ml, $9x10^{10}$ particles/ml) which had an average of 97.5% of microwells. The negative control showed a very low background level of 1.4% of positive microwells. It had all the reagents involved in assay except exosomes and is shown as dashed lines in Figure 28. The decreasing trend of positive microwells was seen as the concentration of exosomes was decreased. The theoretical limit of detection obtained by plugging in the sum of background and three times standard deviation in the line equation and it was 40pg/ml. The dynamic range was obtained, and it was 267pg/ml to 100µg/ml.

(a)

```
Command Window
  Number of positive microwells=
      61
```

(b)

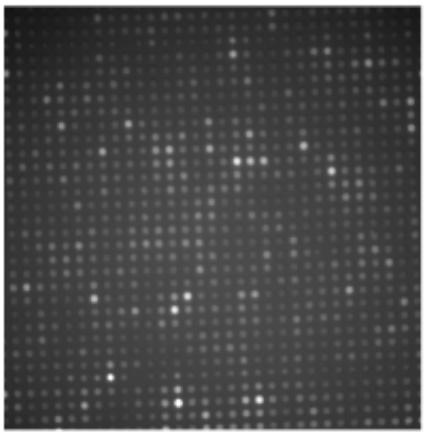

```
Command Window
  Number of positive microwells=
         6728
```

(c)

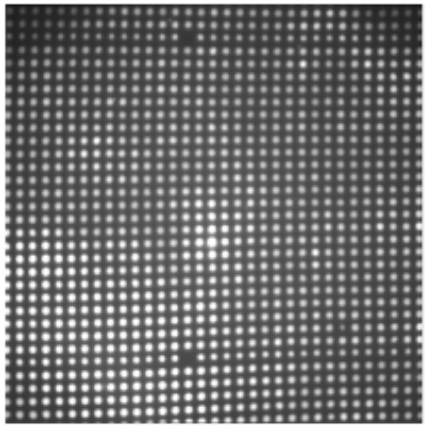

```
Command Window
  Number of positive microwells=
         9909
```

Figure 27: Example of an individual image out of 16 images, covering entire microwell array and their corresponding MATLAB outputs for the entire microarray for (a) Negative control, (b) 10µg/ml (1:100), and (c) 100µg/ml (1:10).

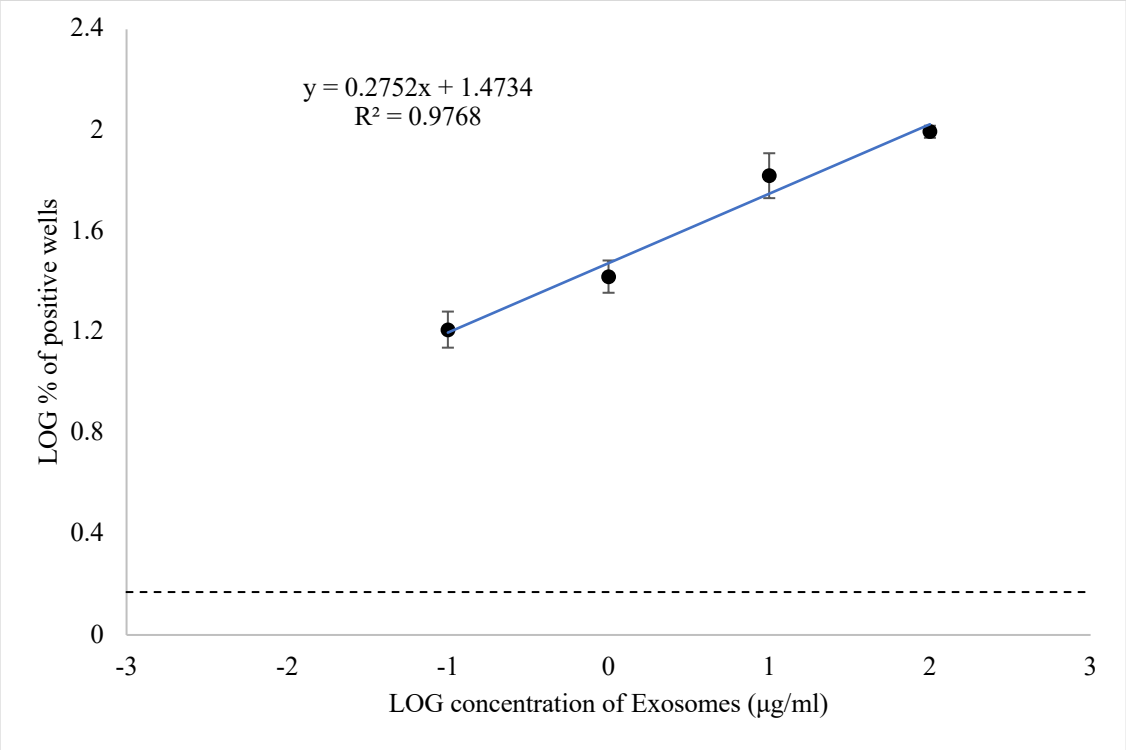

Figure 28: Comparison of log% positive wells vs log concentration of exosomes.

6. Conclusion and Future Work

6.1. Conclusion

Here we successfully developed a microfluidic automated integrated system for extracellular vesicle detection. The closed-loop actuation system was successfully able to seal the microwell array without breaking the chip within a few seconds. It makes it more efficient than a manual sealing manifold or an open-loop actuator without FSR. The master Si molds with SU-8 features were fabricated using photolithography. PDMS chips were cast with the desired features for assay. The quantitative individual detection of EVs was achieved with higher sensitivity. The automated image processing algorithm was able to identify the microwells and analyze individual microwells to count the possibly positive microwells to indicate the presence of EVs. Due to its high accuracy, precision, and efficiency, it shows promising analysis capability for large scale digital assays. Isolating individual EVs in femtoliter microcompartments for analysis paves the path to cutting-edge clinical diagnosis and prognosis techniques.

6.2. Future Work

6.2.1. Standalone Integrated System

By successfully integrating Arduino, FSR, and actuator, an integrated closed-loop system has been built. It can be further extended to include imaging components into the system. Even though microfluidic chips are portable, they still rely on bulky microscopes for imaging. This holds back the ease of portability of these microfluidic chips. Therefore, a camera and a light source can be integrated with the Arduino microcontroller or raspberry pi to build an absolute standalone system. Peristaltic pumps can also be included in the system for sample injection in various steps of the assay. This could completely eliminate human intervention and make it completely automated. As

the algorithm for post image analysis is already successfully completed, it can be easily incorporated into such systems which can output the numbers very fast. It can also be programmed to plot the graphs and output them. By incorporating automation in such assays can significantly reduce the time taken for analysis and help to cope up with the demand for increasing cancer cases.

6.2.2. Digital ELISA

The subsequent step after quantifying the total captured EVs in exosome standard would be to do it for different individual membrane proteins. The assay can be taken to the next step by testing with clinical samples. As the detection antibodies can be varied in the assay, different membrane proteins can be targeted, and quantification of various tumor-associated proteins. Protein profiling of EVs can be done for various targets specific to that particular cancer type. These results can be compared with that of tests run on samples from healthy patients. And to further test the working of the chip, blinded samples can be tested and validated. In the case of blinded samples, any details about the sample will be unknown to the person performing the test.

6.2.3. Detecting Tumor Associated Molecules inside EV

This can be the next step of detecting tumor-associated substances inside EVs after inspecting the membranal proteins. Proteins, microRNAs, or messenger RNAs (mRNAs) can be quantified from the lysate. As the microfluidic chip already has a lysis chamber in it, it can be used to get lysate without diluting it a lot. Magnetic beads immobilized with capture antibodies can be used to capture many EVs onto the beads. They can be localized into the lysis chamber using a magnet (Figure 29). Then it can be lysed by introducing just 0.1µl of lysate by opening the lysis chamber. Then it can be pushed to the diluting chamber and then 0.1µl of dilution buffer can be introduced.

Then they can be mixed and pumped to the detection chamber for detecting molecules of interest. ELISA can be performed if proteins inside are needed to be detected. Or double hybridization can be done to detect microRNAs or mRNAs.

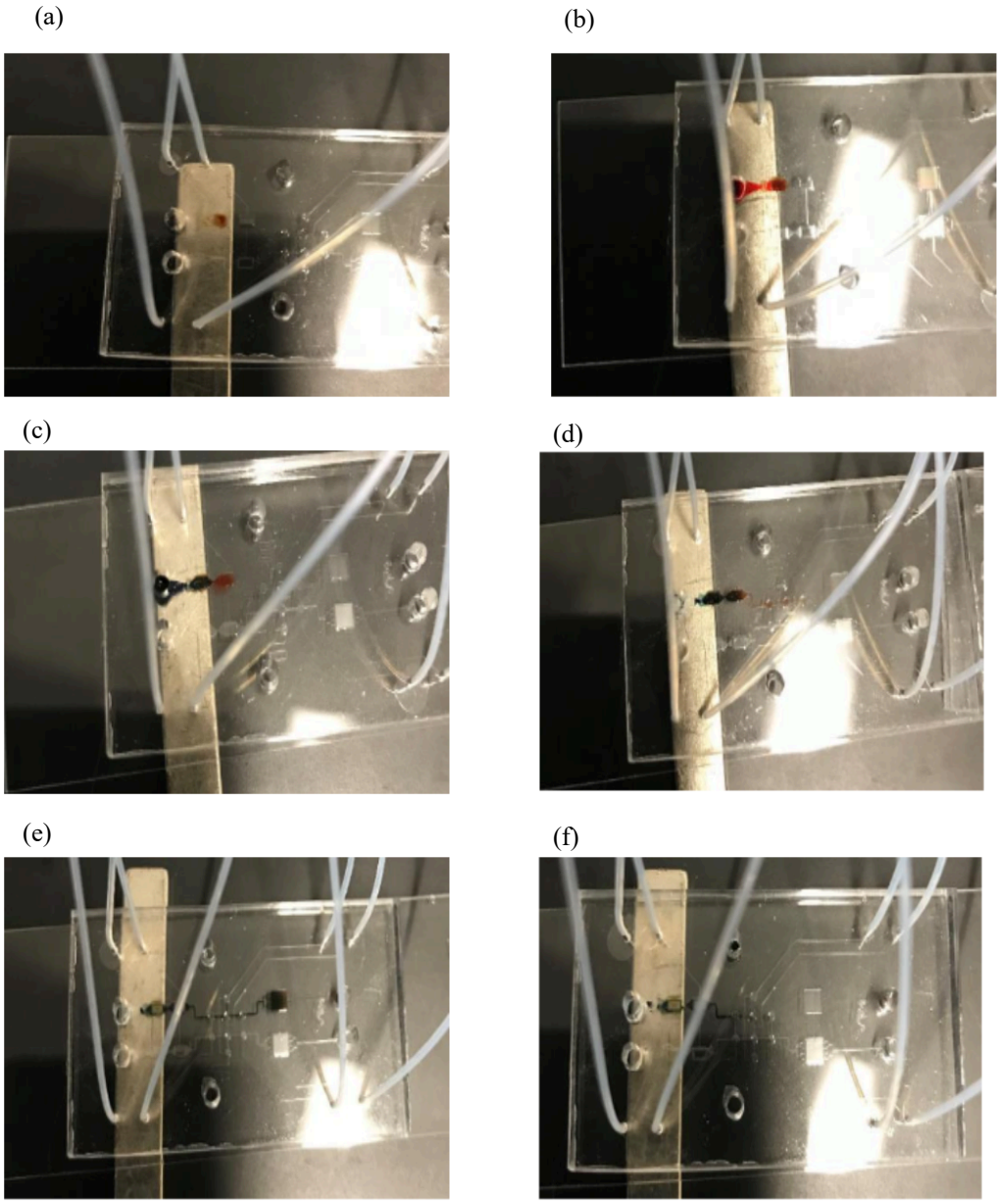

Figure 29: Visualization of the assay protocol using food dyes. (A) Capture of the exosome captured magnetic beads in the lysis chamber. (B) Introduction of the 0.1 µl of lysis buffer(red dye) into the lysis chamber. (C) Dilution of the lysate with dilution buffer(green dye). (D) After dilution of lysate to 0.2 µl. (E) Pumping of the lysate to the detection chamber where capture probes will be immobilized to captute target molecules. (F) Washing the lysate with washing buffer before introducing detection probes.

7. Appendix

7.1. Arduino Code for Closed-loop Actuator

```
#include <Servo.h>

Servo myservo;

int pos;
int pin = 0;
int force;
int fsrReading;
int fsrVoltage;
unsigned long fsrResistance;
unsigned long fsrConductance;
long fsrForce;
void setup()
{
  Serial.begin(9600);
  myservo.attach(7);
  pos=0;
  myservo.write(pos);
  delay(5000);
}

void loop()
{
  fsrReading = analogRead(pin);
  Serial.print("Analog reading = ");
  Serial.println(fsrReading);

 fsrVoltage = map(fsrReading, 0, 1023, 0, 5000);


  if (fsrVoltage == 0) {
    Serial.println("No pressure");
  } else {

    fsrResistance = 5000 - fsrVoltage;
    fsrResistance *= 10000;
    fsrResistance /= fsrVoltage;

    fsrConductance = 1000000;
    fsrConductance /= fsrResistance;


    if (fsrConductance <= 1000) {
      fsrForce = fsrConductance / 80;
      Serial.print("Force in Newtons: ");
      Serial.println(fsrForce);
    } else {
      fsrForce = fsrConductance - 1000;
      fsrForce /= 30;
```

```
      Serial.print("Force in Newtons: ");
      Serial.println(fsrForce);
    }
  }
  Serial.println("--------------------");


if (fsrReading<950)
  {
    pos=pos+1;
    myservo.write(pos);
    delay(150);
  }

 if(fsrReading >940&&fsrReading<950)
  {
    pos=pos;
    myservo.write(pos);
    delay (60UL * 60UL * 1000UL);
    //exit(0);
    pos=0;
    myservo.write(pos);
    delay(100000);


  }
  if(fsrReading >950)
  {
      pos=pos-1;
    myservo.write(pos);
    delay(150);
  }
Serial.print("Position = ");
 Serial.println(pos);

}
```

7.2.MATLAB Code for Detecting and Analyzing Circles

```
clc;
clear all; close all;
counter=0;
ccounter=0;
%% To read individual images of microwell array
for m=1:4
    for n=1:4
rgb = imread("~/path/tile_x00"+m+"_y00"+n+".tif");


%contrast enhanced in Image J to increase detection sensitivity. Used to
%increase sensitivity of detection and to use position data from that to
%use it in original image
```

```
rgb1 = imread("~/path/tile_x00"+m+"_y00"+n+".tif");

% display original image on which the circles will be drawn
figure
 imshow(rgb)

%To find the radius of microwells as pixel values
% [x,y] = ginput(1);
% d = imdistline;


%To delete the imdistline command
% delete(d);

% To find the circles and get the centers and radii data
% [centers, radii] =
imfindcircles(rgb,[9,11],'ObjectPolarity','bright','Sensitivity',0.85,'Method
','twostage','EdgeThreshold',0.012);
% [centers, radii] =
imfindcircles(rgb,[9,11],'ObjectPolarity','bright','Sensitivity',0.935,'Metho
d','twostage','EdgeThreshold',0.007);
[centers, radii] =
imfindcircles(rgb1,[9,12],'ObjectPolarity','bright','Sensitivity',0.89,'Metho
d','twostage','EdgeThreshold',0.012);

%To display images and draw the circles with radius and center data from
detection
imshow(rgb)
h = viscircles(centers,radii);
a=round(centers(:,1));
b=round(centers(:,2));


% average intensity for an area of 6x6 pixels around center
for j=1:length(centers)

           t(j)= (double(rgb(round(centers(j,2)),round(centers(j,1))))
+double(rgb(round(centers(j,2)+1),round(centers(j,1))))
+double(rgb(round(centers(j,2)+2),round(centers(j,1))))
+double(rgb(round(centers(j,2)+3),round(centers(j,1))))
+double(rgb(round(centers(j,2)-1), round(centers(j,1))))
+double(rgb(round(centers(j,2)-2), round(centers(j,1))))
+double(rgb(round(centers(j,2)-3), round(centers(j,1))))
+double(rgb(round(centers(j,2)),round(centers(j,1)+1)))
+double(rgb(round(centers(j,2)),round(centers(j,1)+2)))
+double(rgb(round(centers(j,2)),round(centers(j,1)+2.5)))
+double(rgb(round(centers(j,2)),round(centers(j,1)1)))
+double(rgb(round(centers(j,2)),round(centers(j,1)-1.5)))
+double(rgb(round(centers(j,2)+1),round(centers(j,1)+1)))
+double(rgb(round(centers(j,2)+2),round(centers(j,1)+2)))
+double(rgb(round(centers(j,2)+3),round(centers(j,1)+3)))
+double(rgb(round(centers(j,2)+3),round(centers(j,1)+3)))
+double(rgb(round(centers(j,2)-1),round(centers(j,1)1)))
+double(rgb(round(centers(j,2)-2),round(centers(j,1)-1.5)))
+double(rgb(round(centers(j,2)+1),round(centers(j,1)+2)))
```

```
+double(rgb(round(centers(j,2)+2),round(centers(j,1)+1)))
+double(rgb(round(centers(j,2)+1),round(centers(j,1)+3)))
+double(rgb(round(centers(j,2)+3),round(centers(j,1)+1)))
+double(rgb(round(centers(j,2)+2),round(centers(j,1)+3)))
+double(rgb(round(centers(j,2)+3),round(centers(j,1)+2)))
+double(rgb(round(centers(j,2)+1),round(centers(j,1)+3)))
+double(rgb(round(centers(j,2)+2),round(centers(j,1)+3)))
+double(rgb(round(centers(j,2)+3),round(centers(j,1)+3)))
+double(rgb(round(centers(j,2)+3),round(centers(j,1)+3)))
+double(rgb(round(centers(j,2)-1),round(centers(j,1)+1)))
+double(rgb(round(centers(j,2)-2),round(centers(j,1)+2)))
+double(rgb(round(centers(j,2)-2),round(centers(j,1)+1)))
+double(rgb(round(centers(j,2)-1),round(centers(j,1)+2)))
+double(rgb(round(centers(j,2)-2),round(centers(j,1)-1)))
+double(rgb(round(centers(j,2)-3),round(centers(j,1)-1)))
+double(rgb(round(centers(j,2)+2),round(centers(j,1)-1)))
+double(rgb(round(centers(j,2)+3),round(centers(j,1)-1))));

           t1(j)=(t(j)/36);
end

figure(3);
% % histogram(t1,65535);
xlabel('Intensity');
ylabel('Number of microwells');

%To count the number of positive microwells for each image
for k=1:length(centers)

    if t1(k)>=3200
        counter=counter+1;

    else
        counter=counter;
    end
end
ccounter=ccounter+length(centers);

disp('Number of positive microwells=');
disp(counter);
    end
    disp("Number of microwells"+ccounter)
end
```

7.3. Detection and Analysis of Square Microwells

The contrast-enhanced image and raw image was imported into MATLAB code. The contrast-enhanced image was converted into a black and white image. Using *regionprops* function, the area value, and centroid and bounding box coordinates of detected regions were acquired. By looking into the number of times each area value was repeated, the threshold range for the area was

selected. The regions within the chosen threshold were filtered and displayed in the image (Figure 30). Using the area, the side of the square was calculated. Then, the average intensity of every pixel inside the square was calculated. It was then compared with the manual threshold value to determine if it classified as a positive microwell. The final positive microwell count was displayed in the command window. This algorithm was used in a recent publication from our group where digital PCR for mRNA detection was done[45].

MATLAB code

```
clear all;
close all;
clc;
%contrast enhanced image
rgb1 = imread('filepath');
%raw image
rgb = imread('filepath');
%converting the image to black and white
bw = im2bw(rgb1,0.3);
% find both black and white regions properties
stats = [regionprops(bw)];
%Converting to dataset
stats_Dataset=struct2dataset(stats);
%converting to array
stats_Array_All=double(stats_Dataset);
%first column contains the area
area_Array=stats_Array_All(:,1);
%finding the repeated area values in area
unique_Area=unique(area_Array);
%finding the repetition of each area value
times_Repeated=histc(area_Array,unique_Area);
%plot array
area_Repeated=[unique_Area times_Repeated];
area_Threshold_1=255;%Threshold area
area_Threshold_2=453;%Threshold area
%count for getting elements in between the area threshold
counter_Final_Array=1;
%finding the area threshold elements
for i=1:length(stats_Array_All)

if((stats_Array_All(i,1)>=area_Threshold_1)&&((stats_Array_All(i,1)<=area_Thr
eshold_2)))
        stats_Final_Array_All(counter_Final_Array,:)=stats_Array_All(i,:);
        counter_Final_Array=counter_Final_Array+1;
    end
end
%acquiring the first column
final_Area=stats_Final_Array_All(:,1);
```

```
%rounding off and finding the value of the side of square from diameter
final_side=fix(sqrt(final_Area)/2);
%extracting the centers of the squares
centers=[fix(stats_Final_Array_All(:,2)) fix(stats_Final_Array_All(:,3))];
%drawing box around the square
final_Bounding_Box=[stats_Final_Array_All(:,4) stats_Final_Array_All(:,5)
stats_Final_Array_All(:,6) stats_Final_Array_All(:,7)];
%show the image and draw the detected rectangles on it
imshow(rgb);
hold on;
for j=1:length(centers)
    sum=0;
    x_min=centers(j,2)-final_side(j);
    x_max=centers(j,2)+final_side(j);
    y_min=centers(j,1)-final_side(j);
    y_max=centers(j,1)+final_side(j);
    disp("xmin="+x_min+"xmax="+x_max+"ymin="+y_min+"ymax="+y_max);
    for x=x_min:x_max
        for y=y_min:y_max
           sum= sum+double(rgb(x,y));
        end
    end
    t(j)=sum;
    t1(j)=t(j)/final_Area(j);
end
% end

figure(3);
histogram(t1);
xlabel('Intensity');
ylabel('Number of microwells');
counter=0;

for k=1:length(centers)
    %Threshold value
    if t1(k)>=4600
        counter=counter+1;

    else
        counter=counter;
    end
end

disp('Number of positive microwells=');
disp(counter);
```

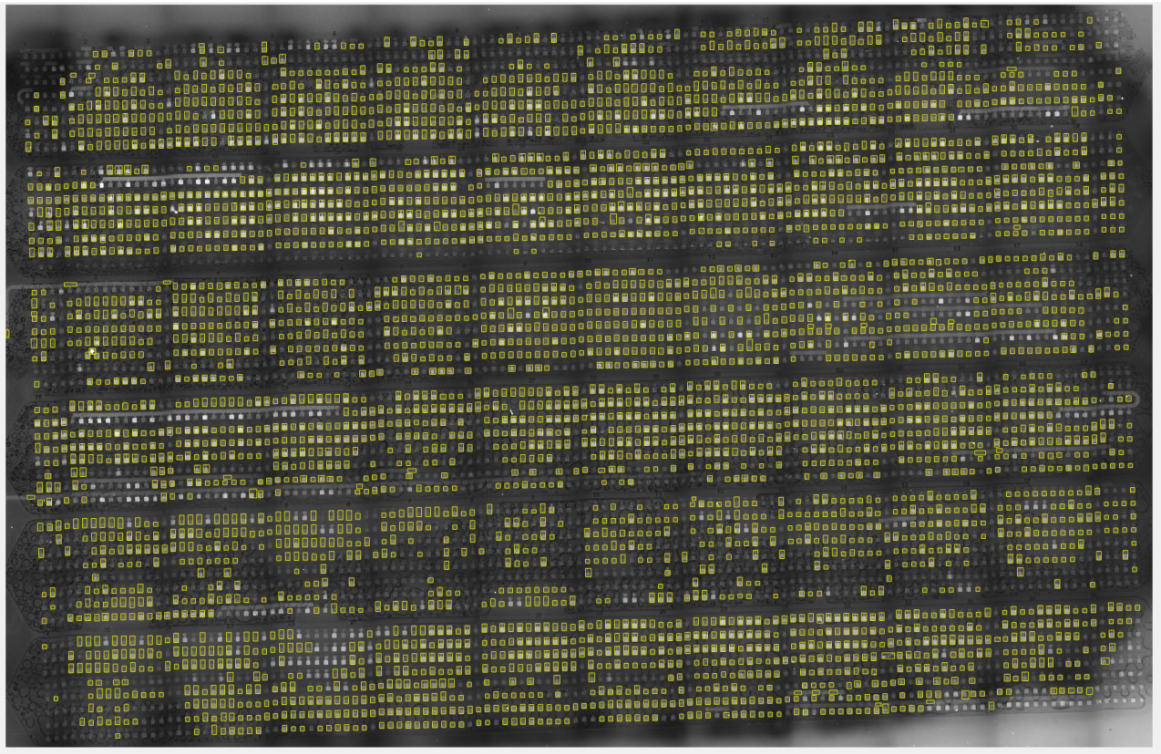

Figure 30: Image showing detected squares in a microarray with square shaped microwells.

Reference

1. Zhang, P., et al., *Ultrasensitive detection of circulating exosomes with a 3D-nanopatterned microfluidic chip.* Nat Biomed Eng, 2019. **3**(6): p. 438-451.
2. Bloemen, M., *Immunomagnetic separation of bacteria by iron oxide nanoparticles.* 2015.
3. *Ada Fruit Learning Sytem. Force Sensitive Resistor Data Sheet.* . 2018.
4. Mathworks, M., *The Mathworks, Inc*. 1993, Boston.
5. Kim, P., et al., *Soft lithography for microfluidics: a review.* 2008.
6. He, M. and Y. Zeng, *Microfluidic exosome analysis toward liquid biopsy for cancer.* Journal of laboratory automation, 2016. **21**(4): p. 599-608.
7. Kim, S.H., et al., *Large-scale femtoliter droplet array for digital counting of single biomolecules.* Lab on a Chip, 2012. **12**(23): p. 4986-4991.
8. Lisensky, G.C., et al., *Replication and compression of surface structures with polydimethylsiloxane elastomer.* Journal of Chemical Education, 1999. **76**(4): p. 537.
9. Prabhakarpandian, B., et al., *Microfluidic devices for modeling cell–cell and particle–cell interactions in the microvasculature.* Microvascular research, 2011. **82**(3): p. 210-220.
10. Rissin, D.M., et al., *Single-molecule enzyme-linked immunosorbent assay detects serum proteins at subfemtomolar concentrations.* Nature biotechnology, 2010. **28**(6): p. 595.
11. Rondelez, Y., et al., *Microfabricated arrays of femtoliter chambers allow single molecule enzymology.* Nature biotechnology, 2005. **23**(3): p. 361-365.
12. Zhang, P., et al., *Ultrasensitive quantification of tumor mRNAs in extracellular vesicles with an integrated microfluidic digital analysis chip.* Lab on a Chip, 2018. **18**(24): p. 3790-3801.
13. Siegel, R.L., K.D. Miller, and A. Jemal, *Cancer statistics, 2020.* CA: A Cancer Journal for Clinicians, 2020. **70**(1): p. 7-30.
14. David, A.R. and M.R. Zimmerman, *Cancer: an old disease, a new disease or something in between?* Nature Reviews Cancer, 2010. **10**(10): p. 728-733.
15. Takeuchi, T., et al., *Antibody-conjugated signaling nanocavities fabricated by dynamic molding for detecting cancers using small extracellular vesicle markers from tears.* Journal of the American Chemical Society, 2020.
16. Zhang, P., M. He, and Y. Zeng, *Ultrasensitive microfluidic analysis of circulating exosomes using a nanostructured graphene oxide/polydopamine coating.* Lab on a Chip, 2016. **16**(16): p. 3033-3042.
17. Andreu, Z. and M. Yáñez-Mó, *Tetraspanins in extracellular vesicle formation and function.* Frontiers in immunology, 2014. **5**: p. 442.
18. Tabeling, P., *Introduction to Microfluidics Oxford University Press*. 2005, Oxford, England ISBN.
19. Choi, K., et al., *Digital microfluidics.* Annual review of analytical chemistry, 2012. **5**: p. 413-440.
20. Janasek, D., J. Franzke, and A. Manz, *Scaling and the design of miniaturized chemical-analysis systems.* Nature, 2006. **442**(7101): p. 374-380.
21. Faley, S.L., et al., *Microfluidic single cell arrays to interrogate signalling dynamics of individual, patient-derived hematopoietic stem cells.* Lab on a Chip, 2009. **9**(18): p. 2659-2664.
22. Murphy, T.W., et al., *Recent advances in the use of microfluidic technologies for single cell analysis.* Analyst, 2018. **143**(1): p. 60-80.

23. Lu, Y., et al., *Rapid prototyping of paper-based microfluidics with wax for low-cost, portable bioassay.* Electrophoresis, 2009. **30**(9): p. 1497-1500.
24. Yeo, L.Y., et al., *Microfluidic devices for bioapplications.* small, 2011. **7**(1): p. 12-48.
25. Zhang, Z. and S. Nagrath, *Microfluidics and cancer: are we there yet?* Biomedical microdevices, 2013. **15**(4): p. 595-609.
26. Raj M, K. and S. Chakraborty, *PDMS microfluidics: A mini review.* Journal of Applied Polymer Science: p. 48958.
27. Toepke, M.W. and D.J. Beebe, *PDMS absorption of small molecules and consequences in microfluidic applications.* Lab on a Chip, 2006. **6**(12): p. 1484-1486.
28. Xia, Y. and G.M. Whitesides, *Soft lithography.* Annual review of materials science, 1998. **28**(1): p. 153-184.
29. Dammel, R., *Diazonaphthoquinone-based resists*. Vol. 11. 1993: SPIE press.
30. Madou, M.J., *Fundamentals of microfabrication: the science of miniaturization*. 2002: CRC press.
31. Franssila, S., *Introduction to microfabrication*. 2010: John Wiley & Sons.
32. Natarajan, S., D. Chang-Yen, and B. Gale, *Large-area, high-aspect-ratio SU-8 molds for the fabrication of PDMS microfluidic devices.* Journal of Micromechanics and Microengineering, 2008. **18**(4): p. 045021.
33. Lequin, R.M., *Enzyme immunoassay (EIA)/enzyme-linked immunosorbent assay (ELISA).* Clinical chemistry, 2005. **51**(12): p. 2415-2418.
34. Engvall, E. and P. Perlmann, *Enzyme-linked immunosorbent assay (ELISA).* Protides of the biological fluids, 1971: p. 553-556.
35. Wild, D., *The immunoassay handbook: theory and applications of ligand binding, ELISA and related techniques*. 2013: Newnes.
36. Coons, A.H., *The demonstration of pneumococcal antigen in tissues by the use of fluorescent antibody.* J Immunol, 1942. **45**: p. 159.
37. DiStefano, J.J., A.R. Stubberud, and I.J. Williams, *Feedback and control systems*. 2012: McGraw-Hill Education.
38. Nageshwar, N., et al. *Thrust Measurement Using Force Sensitive Resistor*. in *2017 IEEE International Conference on Computational Intelligence and Computing Research (ICCIC)*. 2017. IEEE.
39. Shapiro, L.G. and G.C. Stockman, *Computer vision*. 2001: Prentice Hall.
40. Davies, E.R., *Machine vision: theory, algorithms, practicalities*. 2004: Elsevier.
41. Yuen, H., et al., *Comparative study of Hough transform methods for circle finding.* Image and vision computing, 1990. **8**(1): p. 71-77.
42. Gonzalez, R.C. and R.E. Woods, *Image processing.* Digital image processing, 2007. **2**: p. 1.
43. Wang, T., et al., *Ultrasensitive microfluidic solid-phase ELISA using an actuatable microwell-patterned PDMS chip.* Lab on a Chip, 2013. **13**(21): p. 4190-4197.
44. Zeng, Y., M. Shin, and T. Wang, *Programmable active droplet generation enabled by integrated pneumatic micropumps.* Lab on a Chip, 2013. **13**(2): p. 267-273.
45. Zhou, X., et al., *A microfluidic alternating-pull–push active digitization method for sample-loss-free digital PCR.* Lab on a Chip, 2019. **19**(24): p. 4104-4116.